

See discussions, stats, and author profiles for this publication at: <https://www.researchgate.net/publication/257070207>

Mechanism of Iron Carbonyl- Catalyzed Hydrogenation of Ethylene. I. Theoretical Exploration of Molecular Pathways.

ARTICLE in THE JOURNAL OF PHYSICAL CHEMISTRY A · SEPTEMBER 2013

Impact Factor: 2.69 · DOI: 10.1021/jp406878k · Source: PubMed

CITATIONS

2

READS

34

2 AUTHORS, INCLUDING:



Rubik Asatryan

University at Buffalo, The State University of N...

51 PUBLICATIONS 364 CITATIONS

SEE PROFILE

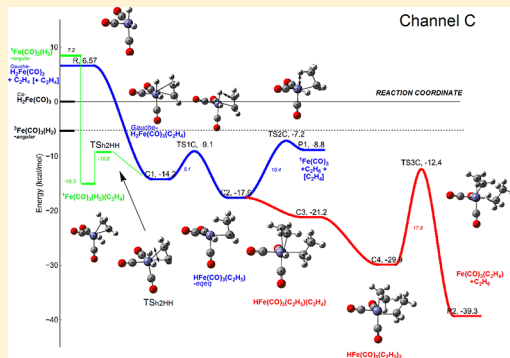
Mechanism of Iron Carbonyl-Catalyzed Hydrogenation of Ethylene. 1. Theoretical Exploration of Molecular Pathways[†]

Rubik Asatryan* and Eli Ruckenstein

Department of Chemical and Biological Engineering, University at Buffalo, State University of New York, Buffalo, New York 14260, United States

Supporting Information

ABSTRACT: The hydrogenation of alkenes catalyzed by metal carbonyls is an intricate process involving reactions of various isomers of labile π - and σ -complexes, hydrides, dihydrides, and their radicals. Two general mechanisms have been suggested in the literature regarding the catalytic hydrogenation of simple alkenes by photochemically activated iron pentacarbonyl: a *molecular* mechanism that involves the sequential replacement of two carbonyl ligands by hydrogen and unsaturated ligands, and a *radical* mechanism involving the EPR-identified iron carbonyl hydride radicals. Even though significant results were obtained in numerous experiments and few theoretical studies, these mechanisms remain phenomenological, without detailed information regarding the potential energy surfaces (PES) and the elementary processes. Several major issues also remain open. It is still unclear, for instance, whether the ethane can be formed via a monomolecular reaction of ethyl hydride isomer intermediates $\text{HFe}(\text{CO})_3(\text{C}_2\text{H}_5)$ or the only way to produce C_2H_6 is a bimolecular reaction assisted by a second ethylene. It is also uncertain if a dihydride or a dihydrogen complex is operating in olefin hydrogenation. To gain insight into these processes, a detailed theoretical examination of various PES for gas-phase reactions of ethylene with potential metallocomplex reagents to primary and secondary products (both singlet and triplet electronic states) was performed using DFT and ab initio methods. Calculations have been carried out for a set of reactions of ethylene with all possible isomers of tricarbonyliron hydrogenates, viz., dihydrides of trans-, cis-, and gauche-configurations (isomers with respect to the two hydridic atoms), and two nonclassical singlet and two triplet dihydrogen complexes, some of them being identified for the first time. The hydrogenation pathways (both molecular and radical) are shown to be strongly stereoselective and dependent on the spin configurations of the initial reagents. The combination of various dihydride isomers with C_2H_4 as separate reaction channels allowed us to explore relevant PES cross sections and to identify corresponding stereoregulated elementary processes. The reaction channels can alternatively start from the association of ethylene with dihydrogen tricarbonyliron complexes and may involve intersystem crossings with triplet pathways, followed by that of the corresponding singlet PES. Various interconversion and isomerization processes involving single-olefin adducts were found to precede the major ethane-elimination reactions (through both monomolecular and second-ethylene-assisted pathways). Monomolecular processes are suggested to occur under appropriate conditions. The stereospecific mechanistic results and thermochemical parameters constitute a basis for developing detailed kinetic models for iron–carbonyl catalysis.



I. INTRODUCTION

Coordinatively unsaturated transition metal (TM) carbonyls are known to catalyze various processes, primarily the hydrogenation, isomerization, and hydroformylation of olefins,^{1–11} C–H bond activation,¹² and Fischer–Tropsch and water–gas-shift reactions.^{4,5,13} Iron carbonyls are widely used in manufacturing new materials and epitaxial layers.¹⁴ $\text{Fe}(\text{CO})_5$ is particularly used in preparation of carbon nanotubes via the catalytic chemical vapor deposition, where molecular hydrogen plays an important role in the growth and microstructure of nanotubes.¹⁵ Iron carbonyls were detected in interstellar dust clouds and other extraterrestrial sources readily interacting with abundant present hydrogen molecules.¹⁶

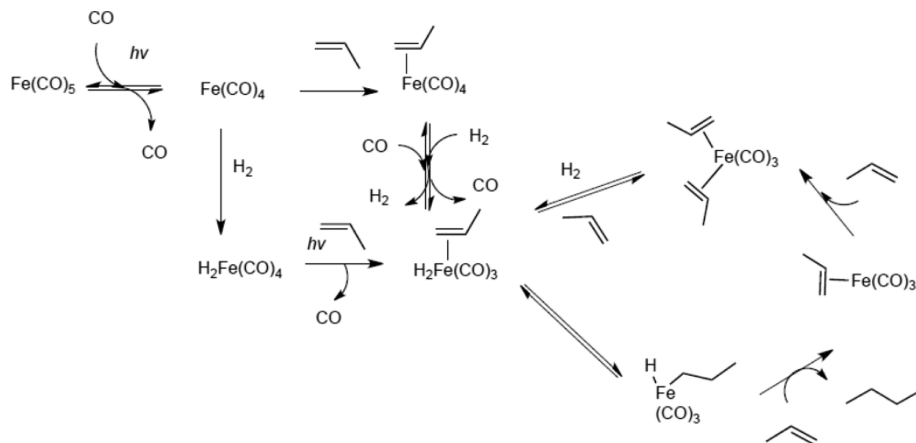
The binding of dihydrogen to organometallic complexes and its activation constitute fundamental steps in many catalytic

mechanisms.^{18–26} In particular, the hydrogenation and isomerization of olefins occur through the thermal and photochemical activation of $\text{Fe}(\text{CO})_5$.^{1,3,5,7,27–46} The thermal processes are relatively slow (for instance, a solution of dienes is hydrogenated only when heated to ca.160 °C under 10 atm H_2 pressures¹⁰), whereas the photoactivated pentacarbonyliron easily generates reactive carbonyl species (photoadducts) and intermediates, thus facilitating these processes.¹ The molecular level mechanism is quite complex because of the interaction of various π - and σ -complexes, hydrides and dihydride intermediates, and radical species through various H-atom transfer,

Received: July 11, 2013

Revised: September 17, 2013

Published: September 24, 2013

Scheme 1. Schroeder–Wrighton's Mechanism for the Liquid-Phase Olefin Hydrogenation Catalyzed by $\text{Fe}(\text{CO})_5$ ²⁸

coordination, and carbonyl-elimination/insertion processes. The UV photolysis of $\text{Fe}(\text{CO})_5$, in the presence of H₂, has been shown to lead to the formation of the dihydride complex $\text{Fe}(\text{CO})_4\text{H}_2$ and also to the nonclassical dihydrogen complex $\text{Fe}(\text{CO})_3(\text{H}_2)$.^{17,32}

Photodissociation dynamics of $\text{Fe}(\text{CO})_5$ and the reactivity of unsaturated iron–carbonyls have been extensively studied and the role of coordinatively unsaturated tri- and tetracarbonyliron species has been outlined (for reviews, see refs 4, 27, 34, and 35 and references cited therein). A substantial amount of ${}^3\text{Fe}(\text{CO})_3$ is created by single-photon absorption of $\text{Fe}(\text{CO})_5$ in solution and its chemistry is suggested to occur in all reactions involving the UV photolysis of $\text{Fe}(\text{CO})_5$.⁴⁷ Combined with the theory of photochemical processes, these studies revealed the main role of the multispin reactivity of iron–carbonyl complexes and intermediates.^{27,42,48,49} It was even suggested that the reagents in a particular spin state can be transformed into products with the same spin state via one or more intermediates of different spins and even a number of spin crossovers. However, the principal role of the classical π -complexes has been emphasized in the reactivity of conjugated systems, predominantly alkenes and dienes.^{32,33}

An inclusive kinetic model is demanding due to the lack of the comprehensive PES data and the problems linked to the multiphase reactivity of metallocomplexes. A few kinetic models have been developed involving phenomenological rate constants and global schemes. The Rice–Ramsberger–Kassel–Marcus (RRKM) theory has been applied to the study of the thermal dissociation of $\text{Fe}(\text{CO})_5$ on the basis of the empirical bond dissociation energies for simple carbonyls.^{50,51} Green and co-workers performed DFT-based detailed quantum RRK kinetic modeling of iron nanoparticle synthesis via the decomposition of $\text{Fe}(\text{CO})_5$.⁵²

Iron carbonyls are key contributors to various iron-based catalytic processes. The exploration of detailed hydrogenation mechanisms of simple olefins provides a quantitative basis for detailed kinetic modeling of both thermal and photochemical processes involved in the catalysis of conjugated organic compounds. To gain insight into the mechanism of these processes, a comprehensive theoretical analysis of the $\text{Fe}(\text{CO})_3$ -catalyzed hydrogenation of ethylene, as the simplest model for olefin hydrogenation, at the level of detailed PES was performed in the present paper.

In 1976, Schroeder and Wrighton proposed a mechanism for the liquid-phase hydrogenation of olefins, which is presented in

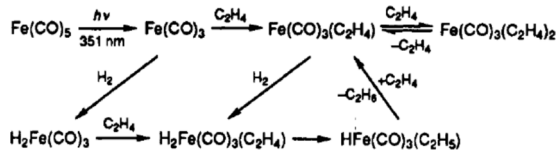
Scheme 1.²⁸ The catalytic cycle involves an olefin coordinated to the dihydridotricarbonyliron complex [$\text{H}_2\text{Fe}(\text{CO})_3(\text{olefin})$] generated via one of two routes, by either the “hydride” or the “olefin” pathway. An intramolecular isomerization of this complex via a H-transfer to the olefin is followed by a free-olefin assisted reductive elimination of the alkane product. The catalytic cycle is completed when a newly generated unsaturated π -complex is combined with a second olefin molecule, followed by the replacement of one of the olefin ligands by H₂. The initial complex $\text{H}_2\text{Fe}(\text{CO})_3(\text{olefin})$ is thus regenerated.

The mechanism of Schroeder and Wrighton has survived experimental tests regarding the intermediates and products. In addition to the $\text{Fe}_2(\text{CO})_6(\text{C}_2\text{H}_4)_2$ intermediate, the 16-electron complex $\text{Fe}(\text{CO})_3(\text{C}_2\text{H}_4)$, which is involved in this mechanism, was identified. The latter compound was formed when an alkene free of allylic hydrogen atom (C₂H₄, pentane, etc.) was presented, whereas the allyl–hydrido complex $\text{HFe}(\text{CO})_3(\pi\text{-allyl C}_3\text{H}_5)$ was formed in the presence of an allylic-H.^{36–40} Note that some actual intermediates might not be detected being operative during the short time scales (see, e.g., refs 11 and 53).

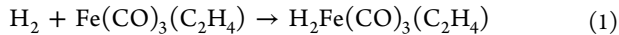
The above general scheme does not include the possible monomolecular alkane-elimination pathway, which might be important particularly for gas-phase processes. The gas-phase bimolecular reaction of a dihydrogen–olefin complex with a free olefin reagent is expected to be less favorable kinetically than the monomolecular reaction. A direct product formation channel is most likely to occur if it involves a *chemically activated* adduct (see, e.g., refs 54–57). These issues require additional exploration.

The mechanism of Schroeder and Wrighton has been further developed in a series of gas-phase kinetic studies, due primarily to Grant, Weitz, and co-workers.^{29–33} The currently accepted reaction scheme is based on the direct observation of the steady-state concentrations of some intermediates, and mostly phenomenological reaction kinetics (Scheme 2^{32,33}). Grant and co-workers hypothesized^{29,31} that the photolytically generated unstable bis-ethylene complex $\text{Fe}(\text{CO})_3(\text{C}_2\text{H}_4)_2$ decomposes thermally by the loss of one ethylene ligand, thus yielding the 16-electron active complex $\text{Fe}(\text{CO})_3(\text{C}_2\text{H}_4)$. A single-ethylene ligated complex provides the entry into the catalytic cycle by a reversible oxidative addition of H₂, which produces the coordinatively saturated complex, $\text{H}_2\text{Fe}(\text{CO})_3(\text{C}_2\text{H}_4)$. It was

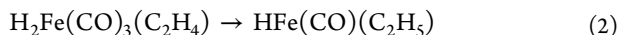
Scheme 2. Current Gas-Phase Mechanism for Olefin Hydrogenation Catalyzed by Photoactivated $\text{Fe}(\text{CO})_5$ ^{29,33}



assumed^{29,30} that a molecular hydrogen reacts with the complex to produce the classical dihydride $\text{H}_2\text{Fe}(\text{CO})_3(\text{C}_2\text{H}_4)$.

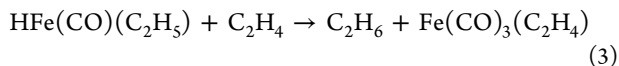


A reversible migratory insertion of a hydride (insertion of ethylene into an Fe–H bond) to form the 16-electron ethyl–hydride complex, $\text{HFe}(\text{CO})_3\text{C}_2\text{H}_5$, constitutes the following step involving $\text{H}_2\text{Fe}(\text{CO})_3(\text{C}_2\text{H}_4)$.



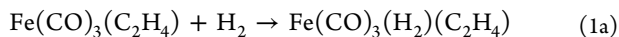
This step was considered to be the rate-determining step in the turnover of the catalytic cycle. Temperature studies indicate an apparent activation energy of 9.4 kcal mol⁻¹, which was assigned to the ethylene insertion reaction. Somewhat lower activation energies were found later by Weitz and co-workers on the basis of thorough kinetic studies of similar processes in the isomerization of propene^{37,39} and 1-pentene³⁸ to form allylmetal–hydride complexes.

A second hydride insertion process driven by ethylene addition takes the cycle back to the catalyst $\text{Fe}(\text{CO})_3\text{C}_2\text{H}_4$ and yields the ethane product.



No direct monomolecular ethane-elimination mechanism was considered in this mechanism, although in a latter study by Weitz's group, a direct reaction has been suggested to occur on the basis of calculated thermochemistry of intermediates (vide infra).⁵⁸

Weitz and co-workers demonstrated that the addition of H_2 to iron carbonyl fragments can yield the “crucial” intermediate $\text{H}_2\text{Fe}(\text{CO})_3(\text{C}_2\text{H}_4)$.^{32,33} The kinetics-based Scheme 2 starts with the reaction of the coordinatively unsaturated $\text{Fe}(\text{CO})_3$ generated in the gas phase via the 351 nm photolysis of $\text{Fe}(\text{CO})_5$.³² Hayes and Weitz observed the formation of the “crucial” intermediate, which was assumed to be a dihydrogen complex, $\text{Fe}(\text{CO})_3(\text{H}_2)(\text{C}_2\text{H}_4)$, in contrast to Grant's suggestion,^{29–31} (eq 1a).

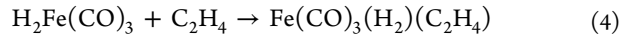


They also assumed that this intermediate undergoes a H-atom-transfer reaction and reductive elimination in the presence of ethylene to yield ethane and regenerate the “catalytic precursor” $\text{Fe}(\text{CO})_3(\text{ethylene})$.³²

Using time-resolved FTIR of UV-photolyzed mixtures of $\text{Fe}(\text{CO})_5$, C_2H_4 , and H_2 , Wells and Weitz monitored the formation of ethane and of two other species, viz., $\text{Fe}(\text{CO})_3(\text{H}_2)(\text{C}_2\text{H}_4)$ and $\text{Fe}(\text{CO})_3(\text{C}_2\text{H}_4)_2$, considering the last two as reservoirs for ethane formation, not in equilibrium with each other. It is noteworthy that the $\text{Fe}(\text{CO})_3(\text{H}_2)(\text{C}_2\text{H}_4)$ intermediate was found to be stable at room temperature, at least during the short (100 μs at room temperature) observation time of their experiment, compared to an ethane

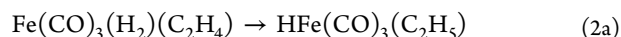
formation time scale of no more than minutes. The latter time scale was explained as due to a modest activation energy.³³

To validate this scheme and completely characterize the kinetics of olefin hydrogenation, it is necessary to determine the rate constants of all relevant reactions. Weitz and co-workers^{32,33} reported direct gas-phase measurements of several rate constants. They monitored the $\text{H}_2\text{Fe}(\text{CO})_3$ complex and the $\text{Fe}(\text{CO})_3(\text{H}_2)\text{C}_2\text{H}_4$ intermediate. The latter species was assumed to be generated from different precursors via the two alternative reactions 1a and 4.



The ethylene-addition reactions were generally found to be faster than the H_2 -addition reactions with a rate constant of formation of bis-ethylene π -complex $\text{Fe}(\text{CO})_3(\text{H}_2)(\text{C}_2\text{H}_4)_2$ the largest among the considered reactions.

In the present PES study we primarily consider the addition of ethylene to $\text{H}_2\text{Fe}(\text{CO})_3$ to generate the catalyst, because of the faster combination reaction 4 compared to the alternative reaction 1.^{32,33} In addition, the stereospecific variations of reaction 4 allowed generating different PES cross sections through structurally diverse intermediates of $\text{H}_2\text{Fe}(\text{CO})_3(\text{C}_2\text{H}_4)$. Notably, the key ethyl hydride intermediate $\text{HFe}(\text{CO})_3\text{C}_2\text{H}_5$, which regenerates after ethane elimination the “catalytic precursor” $\text{Fe}(\text{CO})_3(\text{C}_2\text{H}_4)$ (eq 3), was not observed by Wells and Weitz³³ in their experiments considering it is concentration too small to be detected. The absence of the $\text{HFe}(\text{CO})_3(\text{C}_2\text{H}_5)$ intermediate was interpreted as being either due to a fast reductive elimination of ethane (eq 3) or because the reverse reaction (eq 2a) is very rapid.



One cannot rule out the possibility of the direct ethane elimination from $\text{HFe}(\text{CO})_3(\text{C}_2\text{H}_5)$, which is not involved in Scheme 2. In addition, the $\text{HFe}(\text{CO})_3(\text{C}_2\text{H}_5)$ intermediate can form various π -adducts with a second ethylene. In analogy with reactions 2 it can undergo a second H-transfer (isomerization) reaction, forming a more complex σ -intermediate $\text{Fe}(\text{CO})_3(\text{C}_2\text{H}_5)_2$ (see eqs 6 and 10 in the Results and Discussion). The important role of the π -ligand–metal interactions in the formation and reactivity of conjugated intermediates has also been highlighted by Wells and Weitz,³³ as an alternative to the spin-controlling of such reactions.

Some of the conclusions from the gas-phase mechanism of Grant and co-workers^{29–31} included in Scheme 2, has been challenged by Onda et al. on the basis of the photolysis results on mixtures containing $\text{Fe}(\text{CO})_5$, C_2H_4 , H_2 , and D_2 .⁵⁹ They provided additional information regarding the isomerization of $\text{H}_2\text{Fe}(\text{CO})_3\text{C}_2\text{H}_4$ to $\text{HFe}(\text{CO})_3(\text{C}_2\text{H}_5)$, eq 2. On the basis of the observed statistical distribution between 1,1- d_2 and 1,2- d_2 ethane products, they concluded that a rapid hydrogen atom migration between the carbon atoms at the iron center takes place.

To explain the observed hydrogen scrambling, they assumed that the hydrogen insertion step into ethylene is a reversible process. It was speculated that hydrogen binds to ethyleniron tricarbonyl $\text{Fe}(\text{CO})_3(\text{C}_2\text{H}_4)$ to form, not a dihydride (as suggested by Grant et al.^{29–31}) but a dihydrogen ($\eta^2\text{-H}_2$) molecular complex. This proposition is consonant with the conclusions of Weitz and co-workers noted above.⁵⁸ The scrambling occurs through a rapid series of ethylene insertion–methyl rotation–reverse insertion–ethylene rotation sequences.

However, the absence of detailed PES information did not allow Onda et al. to distinguish conclusively the form of hydrogen complex that accommodates this insertion. It can be either a classical dihydrido complex or a molecular dihydrogen complex.⁵⁹ As shown below, both structures are relevant and operative depending on the symmetry of reagents and intermediates.

The results of Onda et al. demonstrated that deuterated ethanes are produced during the primary hydrogenation process and that one ethylene molecule reacts with one hydrogen molecule on the metal center.⁵⁹ They also confirmed the concept that the hydrogenation reaction takes place as an *intramolecular rearrangement of an iron complex containing both reactants* to form an alkyl–hydrido complex, followed by alkane elimination.

The main consequence of irradiation is to generate different types of highly reactive, often vibrationally excited, organometallic species important in the catalytic behavior of iron carbonyls. In this regard, the free radical intermediates are expected to play an important role in hydrogenation reactions. It would particularly explain the formation of 1,2-*d*₂ ethane in deuterated experiments.

An alternative *radical* mechanism has been proposed by Nagorski and Mirbach, whereby the hydridic radicals play a decisive role.⁶⁰ The hydrogenation of octene catalyzed by iron pentacarbonyl under UV excitation was suggested to occur via the reactions of [HFe(CO)₄][•] radical formed through the secondary processes involving the primary [Fe(CO)₄][•] radicals. They provided evidence that photochemical reaction proceeds via a radical mechanism, because the [HFe(CO)₄][•] radical, the active hydrogenation catalyst, and some other related radicals could be detected under typical hydrogenation conditions^{49,60,61} (also believed to be important in hydroformylation processes⁶⁰). Our detailed calculations, the topic of a separate publication (part 2 of this paper), show that radical reactions occur with fairly low activation energies and should be included when the rate laws and detailed kinetic schemes are derived.

The above minireview clearly shows that the iron–carbonyl catalyzed hydrogenation is an intricate process with several important questions remaining open. Detailed PES studies are essential in identifying the accurate elementary reaction mechanisms. To the best of our knowledge, there are no comprehensive studies in this area. The only relevant calculations have been performed by Weitz et al.⁵⁸ using the BP86 DFT functional on the bonding and geometries of H₂Fe(CO)₃, H₂Fe(CO)₃(C₂H₄), and HFe(CO)₃(C₂H₅) species. It was particularly concluded that H₂Fe(CO)₃ and H₂Fe(CO)₃(C₂H₄) are triplet and singlet dihydrogen complexes, respectively. The latter complex has been suggested to undergo a direct reductive ethane elimination via the ethyl hydride intermediate HFe(CO)₃(C₂H₅). However, the only identified ethyl hydride isomer HFe(CO)₃(C₂H₅), considered as a key intermediate and containing an agostic (C–H···metal) bond,⁵⁸ appears to be a high-energy isomer among several more stable ethyl–hydrido complexes with much stronger (and stereochemically more relevant) agostic interactions, as follows from our detailed PES calculations. The high-energy ethyl hydrido intermediate (higher than that of dihydrogen complex by 10 and 12 kcal mol⁻¹ at the BP86 and B3LYP levels, respectively⁵⁸) is irrelevant because of the expected even higher kinetic barrier of activation for hydrogenation. On the other hand, newly identified ethyl hydride intermediates provide new lower energy pathways. A terminal H-atom of ethylene in these

intermediates serves as an “agostic ligand”, which increases the symmetry and the stability of the Fe polyhedron. It primarily completes a vacant position in the truncated polyhedron of *O*_h local symmetry around the iron-center (*vide infra*).

Despite the limitations in calculated results and the absence of the information about the reaction barriers, Weitz et al. provided some significant conclusions concerning the general mechanism of hydrogenation. In particular, the reductive elimination of ethane from HFe(CO)₃(C₂H₅) in photochemical pentacarbonyliron-catalyzed hydrogenation of ethane has been suggested to proceed *without the addition of a second ethylene unit*.⁵⁸ It was concluded that, although ethylene addition may occur in concert with, or after elimination of ethane, it is not necessary for the elimination of ethane to be exothermic.

In summary, in spite of some significant mechanistic suggestions, no systematic and comprehensive results at the level of detailed potential energy surfaces are available on hydrogenation of olefins by iron carbonyls. Such information is especially important because of the diversity of isomeric reagents and intermediates with different electronic states and conformations. The scarce theoretical studies were limited to the calculations of equilibrium structures, mostly local minima on the corresponding pathways. A comprehensive PES study of olefins and related systems can provide a unified detailed reaction scheme that involves both molecular and radical reaction pathways important for hydrogenation of unsaturated systems by transition metal complexes involving carbonyl ligands. It is essential to elucidate the molecular mechanism at the level of symmetry-specific elementary reactions, and develop a kinetic model which allows predictions of macroscopic results.

The following considerations constitute the first part of a comprehensive theoretical examination of the PES hydrogenation of the simplest olefin (ethylene) catalyzed by the unsaturated iron carbonyls, involving reactions between molecular species, whereas free radical pathways will constitute the topic of a separate publication. In this paper we report the mechanism of formation and subsequent reactions of hydrogenated isomeric complexes of tricarbonyliron with ethylene, H₂Fe(CO)₃(η²-C₂H₄), using various DFT and ab initio methods.

The entrance channels of PES involve the coordination of ethylene with known and novel metallocomplex reagents, namely, the classical dihydrides and dihydrogen complexes of Fe(CO)₃ in both singlet and triplet spin states. The paper is organized as follows. Details of the employed methodology are presented in section II followed by the analysis of four cross sections of PES corresponding to four main reaction channels denoted as A, B, C, and D (section III). Then, a summary of the PES results as well as concluding remarks are presented.

II. COMPUTATIONAL DETAILS

The traditional DFT functionals, such as hybrid B3LYP^{62–64} and B3PW91,^{62,65} and nonhybrid BP86,⁶⁵ have been well tested regarding the reactivity of iron–organic systems.^{25,42,47,66–80,86} For this reason these methods were employed to perform a comprehensive analysis of the stereospecific hydrogenation processes catalyzed by iron carbonyls.

Previously, the accuracy of these functionals in predicting the energy barriers of simple dihydrogen-catalysis reactions and various models of *nitrogenase* was examined. It was concluded on the basis of a comparison with CCSD(T)/CBS +

Table 1. Relative Energies (ΔE)^a of Tricarbonyliron Hydrogenates at Different Calculation Levels, in kcal mol⁻¹

system	B3LYP(I) ^b	B3LYP(II) ^c	CCSD(T) ^d	B3PW91** ^e	BP86(II) ^c
³ Fe(CO) ₃ (H ₂)-angular ^g	-9.08	-4.88	-5.81	1.4	4.27
³ Fe(CO) ₃ (H ₂)-planar ^h	-9.70	-5.07	-3.35		4.99
cis-H ₂ Fe(CO) ₃	0.0	0.0	0.0	0.0	0.0
gauche-H ₂ Fe(CO) ₃	7.07	6.57	6.50		6.94
Fe(CO) ₃ (H ₂)-angular ^g	4.61	7.20	9.49	6.2	5.98
Fe(CO) ₃ (H ₂)-planar ^h	8.93	10.01	15.80	16.3	f
trans-H ₂ Fe(CO) ₃	12.05	11.18	14.73		f
trans- ³ H ₂ Fe(CO) ₃	15.44	13.11	8.18		20.88

^aAll energies are relative to cis-H₂Fe(CO)₃ isomer + 2C₂H₄, with zero-point vibration energy corrections included. ^bStandard LanL2DZ basis set implemented in Gaussian03 (ref 84). ^c6-311+G(2d,p) triple- ξ basis set for C, H, and O atoms, and LanL2DZ ECP for Fe. ^dSingle-point calculations using B3LYP geometries and zero-point vibration energies, using ECP for Fe and 6-311+G(2d,p) basis set for light atoms. ^eUsing 10% reduced exact exchange energy contribution (ref 49). ^fOptimization converges to cis-H₂Fe(CO)₃ isomer. ^gContains an angular Fe(CO)₃ core. ^hContains a planar Fe(CO)₃ core.

ZPE(CCSD(T))/ aug-pVTZ ab initio benchmark results that the potential energy profiles of model reactions are more accurate at the B3LYP and B3PW91 hybrid levels than at the level of pure GGA BP86 functional.^{25,26} In addition, Albright, Fujimoto, and co-workers demonstrated in a comprehensive stereochemical study that the B3LYP results are much more consistent than MP2/MP4 and CCD ab initio methods for octahedral iron tetracarbonyl dihydrides.⁸⁰ On the other hand, BP86 was found to be more accurate for frequency analysis of the solution chemistry of Fe(CO)₃.⁴⁷ Weitz and co-workers found the BP86 functional to be suitable for the thermochemistry of isomerization and hydrogenation reactions of olefins.^{39,58} In addition, it was shown that the smaller contribution of the exact exchange potential in these functionals results in more correct predictions of the singlet–triplet energy gap for Fe(CO)₄.^{49,76} A modified in this way B3PW91 functional has been particularly employed to study the chemistry of Fe(CO)₅ photoproducts and the oxidative addition of H₂ to Fe(CO)₄.^{17,49}

However, the individual DFT methods have some limitations in evaluating the absolute values of the enthalpies of the formation of organic molecules and metallocomplexes when atomization energy based approaches are used.^{66,68,81} This is in contrast to those based on isodesmic reaction procedures (relative values), which benefit from error compensation, as was also stressed earlier in a detailed analysis.⁸¹ Therefore, the above-mentioned hybrid functionals are suitable for the examination of complex mechanisms and comprehensive PES studies.^{68–74,80,81} It is worth noting that B3LYP results were particularly successful in predicting the bond dissociation enthalpies of formation and dissociation of the significant for the current work species, Fe(CO)₃ and Fe(CO)₄, providing the closest results to CCSD(T) predictions.⁴⁵ It is also known that B3LYP method somewhat overestimates the stability of higher spin multiplicity states^{68–74,79} but provides accurate energies for simple TM complexes, which usually are in high-spin in their ground states.^{65–67}

Consequently, all methods are suitable for mechanistic analysis; however, they are more useful when alternative methods are involved. For this reason we employed B3LYP functional for the initial screening of PES, and the key results were reexamined using the above indicated two hybrids and a GGA DFT as well as the ab initio methods. The initial calculations were performed using the Dunning–Hay double- ζ basis set⁸² and the Los Alamos effective core potential (ECP)

for Fe (the scalar relativistic LanL2DZ basis set),^{83,85} as implemented in Gaussian-03.⁸⁴

The B3LYP hybrid DFT method combines the nonlocal Hartree–Fock exchange functional and corrective terms for the density gradient, developed by Becke⁶² with the LYP correlation functional of Lee et al.,⁶³ as recommended by a group of Gaussian coauthors.⁶⁴ The standard B3LYP/LanL2DZ method involving the double- ξ (D95) basis set on light atoms, is a cost-effective, convergent, and yet fairly consistent method useful for the location of stationary points. It has been used initially in the present paper for the screening of PES, and then the basis sets on C, H, and O atoms were extended using the 6-311+G(2d,p) triple- ξ basis set, which includes diffuse functions to account for long distance interactions, and polarization functions to treat properly the flexible angular charge distributions. All PES results and energy profiles are presented at the same B3LYP/LanL2DZ/6-311+G(2d,p) level to allow comparison of the results, whereas selected more precise or alternative calculation results for somewhat doubtful stationary points are specified in the text. Key stationary points were refined at the CCSD(T)/LanL2DZ/6-311+G(2d,p) single-point level using the geometries and zero-point vibration corrections computed at the B3LYP level (with the same basis set), which are generally known to be accurate.^{68–74} Some comparative results are presented in Table 1.

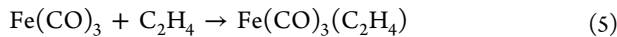
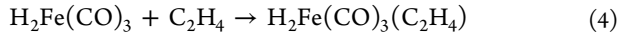
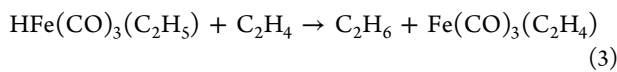
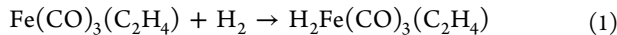
The PES stationary points were characterized using numerical frequency analyses (the TS modes are sketched in the relevant figures for clarity). No symmetry restrictions were applied in the calculations. The intrinsic reaction coordinate (IRC) procedure is employed to identify the connectivity between the stationary points across the PES. The final scanning point structures were fully optimized to ensure that a reaction through the saddle point leads to the proper reactants and products. The effect of an ultrafine grid was considered for typical reactions with no noticeable improvements in the results. The effect of basis set superposition error (BSSE) was not included. It was expected to be insignificant for key monomolecular interconversion processes.

All energy barriers calculated in this paper, denoted $\Delta E^{\#}$, are based on the electronic energy corrected for the zero point vibration energy, calculated at the same level of theory, unless otherwise stated.

III. RESULTS AND DISCUSSION

According to the general mechanism of olefin hydrogenation, discussed in the Introduction (Scheme 2), the main catalytic

cycle of hydrogenation involves a molecular reaction network 1–3, whereas reactions 4 and 5 regenerate alternatively the catalyst (repeating unit), $\text{H}_2\text{Fe}(\text{CO})_3(\text{C}_2\text{H}_4)$, and form the precatalyst π -complex $\text{Fe}(\text{CO})_3(\text{C}_2\text{H}_4)$, respectively.^{29–33,58,59}



The ethylene hydrogenation takes place via the initial ligation of a dihydride/dihydrogen tricarbonyl reagent [$\text{H}_2\text{Fe}(\text{CO})_3$] by the alkene (eq 4). It forms the dihydridotricarbonyliron catalyst, which subsequently reacts to produce ethane (eqs 2 and 3). This pathway is similar to the known “hydride” route for olefin hydrogenation using Wilkinson’s catalyst, $\text{RhCl}(\text{PPh}_3)_3$.^{11,53,76,77} The intermediate-catalyst $\text{H}_2\text{Fe}(\text{CO})_3(\text{C}_2\text{H}_4)$ can be alternatively formed via reaction 5, followed by the precursor formation reaction 1, the reminiscence of the “olefin” route of the hydrogenation catalyzed by a cationic metallocomplex.¹¹ The hydridic H-migration to the olefin (formation of a σ -complex via ethylene insertion into the Fe–H bond via eq 2), followed by a second ethene (free or bath reagent)-assisted reductive elimination of ethane (eq 3), complete the main catalytic cycle. Whereas the above reaction scheme is commonly accepted, it remains phenomenological and does not include detailed elementary reactions, as emphasized by Weitz and co-workers.⁵⁸ The real process appears to be much more complex, as shown below. This paper is concentrated on the stereospecific variations in reaction 4 and subsequent transformations.

The main focus of the present paper is to study the detailed elementary processes involved in the hydrogenation of ethylene after its combination with various hydrogenated tricarbonyliron reagents. This is the most important and controversial part of the current mechanism (see the Introduction). In this regard, we identified the most relevant dihydridotricarbonyliron isomers and demonstrated that they react with ethylene in many ways, which are illustrated in Figures 1–7. The diversity of the initial reactions and discrimination of entrance channels of PES allowed us to explore the most significant monomolecular interconversion processes leading to the final products.

We have not explored in detail the association reaction 4 itself, which is generally known to be a low-barrier (or even a barrierless³) process, but rather studied the diversity of the subsequent processes. To describe the rate constants of such reactions (typically “unactivated”, as noted by Weitz et al.³) it is necessary to employ the variational transition-state theory. Notably, the association reaction may alter the singlet–triplet crossover rates, which also must be considered. A detailed kinetic model based on the mechanisms suggested in the present and subsequent papers on radical reactions is in progress.

The association step typically generates an isomeric hydrogenated π -complex $\text{H}_2\text{Fe}(\text{CO})_3(\eta^2\text{-C}_2\text{H}_4)$, as key intermediate, which undergoes various transformations followed by two characteristic pathways of ethane formation via two general transition states, denoted TS2*i* and TS3*i*, where *i* indicates one

of the channels denoted as A, B, C, or D (vide infra). Interconversions primarily involve the olefin insertion into a Fe–H bond; in other words, a hydridic H-atom is transferred to the olefin via the transition-state TS1*i* (Figure 2). Other isomerization processes necessary to form suitable prereaction complexes for subsequent reductive-elimination reactions involve the internal rotations of ethylene π -ligands, and nonclassically ligated hydrogen molecules, as well as newly formed coordinatively bound ethyl groups.

Four major reaction channels were particularly identified in the present paper (A, B, C, and D) that differ in the manner in which they originate from three distinct singlet-state dihydrides. The corresponding PES cross sections are illustrated in Figures 2, 4, 6, and 7 and the relative energies are presented in Tables 2–5. Channels A and B start with the ethylene coordination to

Table 2. Relative Energies (ΔE) and Enthalpies (ΔH) of Stationary Points along PES Cross-Section A^a (Channel A), in kcal mol^{−1}

species	ΔE	$\Delta H(298\text{K})$
${}^3\text{H}_2\text{Fe}(\text{CO})_3 + 2\text{C}_2\text{H}_4$	13.11	14.12
<i>trans</i> - $\text{H}_2\text{Fe}(\text{CO})_3 + 2\text{C}_2\text{H}_4$	11.18	11.47
$\text{Fe}(\text{CO})_3(\text{H}_2) + 2\text{C}_2\text{H}_4$	10.01	10.28
<i>cis</i> - $\text{H}_2\text{Fe}(\text{CO})_3 + 2\text{C}_2\text{H}_4$	0.0	0.0
${}^3\text{Fe}(\text{CO})_3(\text{H}_2) + 2\text{C}_2\text{H}_4$	−5.07	−4.17
<i>trans</i> - $\text{H}_2\text{Fe}(\text{CO})_3(\eta^2\text{-C}_2\text{H}_4) + \text{C}_2\text{H}_4$	−5.00	−5.67
$\text{HFe}(\text{CO})_3\text{C}_2\text{H}_5\text{-eqax} + \text{C}_2\text{H}_4$	−21.30	−22.15
$\text{TS}_{\text{rotA}} + \text{C}_2\text{H}_4$	−10.15	−11.03
$\text{HFe}(\text{CO})_3\text{C}_2\text{H}_5 + \text{C}_2\text{H}_4$	−12.90	−13.29
$\text{TS2A} + \text{C}_2\text{H}_6 + \text{C}_2\text{H}_4$	−2.08	−2.65
$\text{Fe}(\text{CO})_3 + \text{C}_2\text{H}_6 + \text{C}_2\text{H}_4$	−8.83	−8.75
${}^3\text{Fe}(\text{CO})_3 + \text{C}_2\text{H}_6 + \text{C}_2\text{H}_4$	−29.10	−29.22
$\text{HFe}(\text{CO})_3(\text{C}_2\text{H}_5)(\eta^2\text{-C}_2\text{H}_4)$	−25.84	−26.96
TS3A	−12.70	−13.85
$\text{Fe}(\text{CO})_3(\eta^2\text{-C}_2\text{H}_4) + \text{C}_2\text{H}_6$	−39.26	−39.78
${}^3\text{Fe}(\text{CO})_3(\eta^2\text{-C}_2\text{H}_4) + \text{C}_2\text{H}_6$	−47.61	−47.41

^aAll energies are relative to the *cis*-dihydride isomer, *cis*- $\text{H}_2\text{Fe}(\text{CO})_3$ calculated at B3LYP/LanL2DZ[Fe]/6-311+G(2d,p) [C,H,O] level. Zero-point vibration energies are included.

trans- $\text{H}_2\text{Fe}(\text{CO})_3$ and *cis*- $\text{H}_2\text{Fe}(\text{CO})_3$ dihydridotricarbonyliron isomeric complexes, respectively, whereas channels C and D start from the same *gauche*- $\text{H}_2\text{Fe}(\text{CO})_3$ configuration (the isomers are designated with respect to the two hydridic H-atoms, viz., the H–Fe–C–H dihedral angles). Once the olefin insertion step (the H-transfer process) via transition-state TS1C/D is achieved, branching occurs, leading to different sets of product formation pathways.

In addition, we identified a high-energy triplet tricarbonyliron dihydride with a trans-disposition of the hydridic atoms. According to B3LYP results this isomer is located at a somewhat higher energy (by 2 kcal mol^{−1}) than its singlet counterpart (Table 1), in agreement with the results of Besora et al. calculated at B3PW91* DFT level using a reduced exchange-HF potential.⁴⁹ Even though our CCSD(T) results predicted more stability of this isomer (Table 1), the triplet isomer was not considered as a separate reaction channel because of the repulsive character of the triplet PES, rather it was included in channel A as an alternative reagent (Figure 1).

Besora et al. reported four isomers of the [$\text{H}_2\text{Fe}(\text{CO})_3$] system when studying the hydrogenation of tricarbonyliron complexes, namely, the singlet *cis*- $\text{H}_2\text{Fe}(\text{CO})_3$ and the triplet

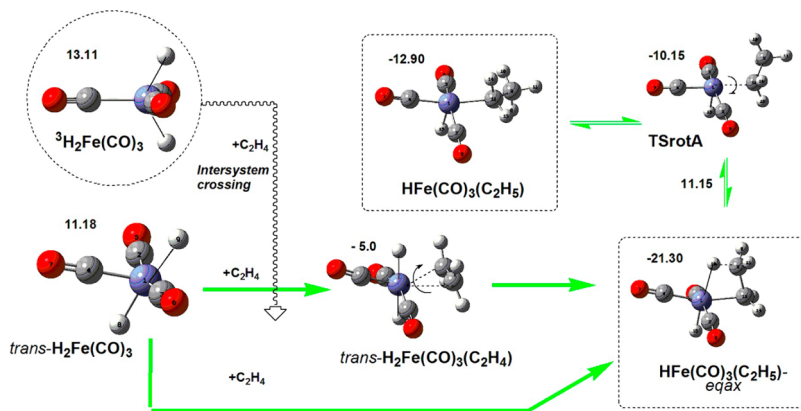


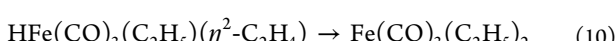
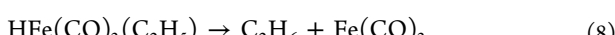
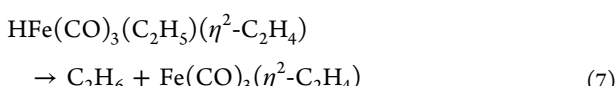
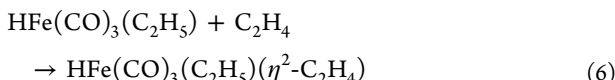
Figure 1. Initial steps in channel A involving the formation and interconversion of olefin π -complexes and hydrido–alkyl σ -complexes. The numbers above the structures (in kcal mol^{-1}) indicate the stabilities relative to cis-isomer, whereas the barrier heights are indicated on the arrows. Two ethyl hydride adducts and a triplet reagent, are outlined.

trans- $\text{H}_2\text{Fe}(\text{CO})_3$ dihydrides and triplet and singlet dihydrogen $\text{Fe}(\text{CO})_3(\text{H}_2)$ complexes.⁴⁹ Instead, we identified eight isomers presented in Table 1 (Cartesian coordinates are provided in Supporting Information).

The key ethylene dihydride intermediate ($\text{H}_2\text{Fe}(\text{CO})_3(\eta^2\text{-C}_2\text{H}_4)$) can be alternatively generated via the coordination of H_2 to the π -complex $\text{Fe}(\text{CO})_3(\eta^2\text{-C}_2\text{H}_4)$, as considered in eq 1 and Scheme 2. This reaction regenerates the catalytic cycle once the TS3i barrier is surmounted and ethane is produced (eq 3). However, reaction 1 is somewhat slower (by a factor of 1.4, as determined by Weitz and co-workers^{32,33}) than the basic ethylene coordination reaction 4, employed in the current paper as the entrance channel of PES.

The “crucial” intermediate $(\text{H}_2\text{Fe}(\text{CO})_3(\eta^2\text{-C}_2\text{H}_4)$ or $\text{H}_2\text{Fe}(\text{CO})_3(\eta^2\text{-C}_2\text{H}_4)$ can also be formed either via the coordination of C_2H_4 with a singlet dihydrogen complex $\text{Fe}(\text{CO})_3(\text{H}_2)$, in a spin-allowed reaction, or via the reaction of the triplet dihydrogen complex, ${}^3\text{Fe}(\text{CO})_3(\text{H}_2)$, in a spin-forbidden reaction. However, in the latter case the spin-crossing with both the singlet $\eta^2\text{-H}_2$ - and dihydrido pathways must occur to advance the process, because the triplet-state PES appears to be mostly repulsive (vide infra). Both processes then merge with the original PES of the singlet dihydride.

The overall catalytic process can be now supplemented by general eqs 6–10 on the basis of calculation results.



These general equations combine the actual symmetry-specific elementary reactions, which are identified on the corresponding PES cross sections (Figures 2, 4, 6, and 7). Reactions 6 and 7 involve the formation and decomposition of ethyl monohydrido–ethylene π -complex intermediate and provide details of the global reaction 3, whereas reaction 8

provides information regarding the direct monomolecular elimination of ethane. The direct reductive elimination generates also a singlet $\text{Fe}(\text{CO})_3$ as a coproduct, which can subsequently associate with a hydrogen molecule (eq 9) to form an isomer of $[\text{H}_2\text{Fe}(\text{CO})_3]$, and thus the catalytic cycle is repeated. A singlet–triplet crossover may also occur in the final stages of the overall reaction which produces the triplet ${}^3\text{Fe}(\text{CO})_3$. The novel π -complex $\text{HFe}(\text{CO})_3(\text{C}_2\text{H}_5)(\eta^2\text{-C}_2\text{H}_4)$ not only undergoes a reductive elimination via reaction 7 but also can feasibly isomerize via eq 10 to form a new σ -complex $\text{Fe}(\text{CO})_3(\text{C}_2\text{H}_5)_2$, as in reaction 2. $\text{Fe}(\text{CO})_3(\text{C}_2\text{H}_5)_2$ can be considered as the dialkyl analogue of the dihydride, $\text{H}_2\text{Fe}(\text{CO})_3$. These reactions will be discussed in more detail in section 3.5.

The olefin coordination to dihydride/dihydrogen tricarbonyliron complexes generates various π -complexes, isomers with different potential energy profiles. Thus, the conformation and symmetry of the initial reagents introduces diversity in the reaction profiles (PES cross sections).

As seen from Figures 2, 4, 6, and 7, the monomolecular reaction pathways through TS2i are generally more energy demanding, than those via TS3i. Yet, they are feasible for some channels, depending on the intramolecular rearrangements of adduct intermediates. The direct reductive elimination of ethane may occur especially when the prereaction adducts are energized either via the photon absorption/vibrational-excitation-energy redistribution^{4,5} or via chemical activation.^{55–57} The combination of reagents in the latter case provides a much lower energy adduct, thus gaining internal energy, which allows surmounting the intrinsic barriers. Bimolecular pathways through TS3i form ethane via a second-ethylene-addition mechanism (eqs 6 and 7), being mostly low-energy processes.

The interconversion processes (primarily H-transfer and internal rotation of ethyl groups and $\text{C}_2\text{H}_4/\text{H}_2$ ligands) were found to play a significant role in the seemingly simple reductive elimination of ethane. Importantly, the isomerization processes may provide the rate-determining step and should be explicitly taken into account in the development of inclusive kinetic models. The obvious advantage of the gas-phase monomolecular processes involving interconversions and reactions via TS2i is that they are more entropically (dynamically) controlled as opposed to bimolecular reactions which occur via TS3i.

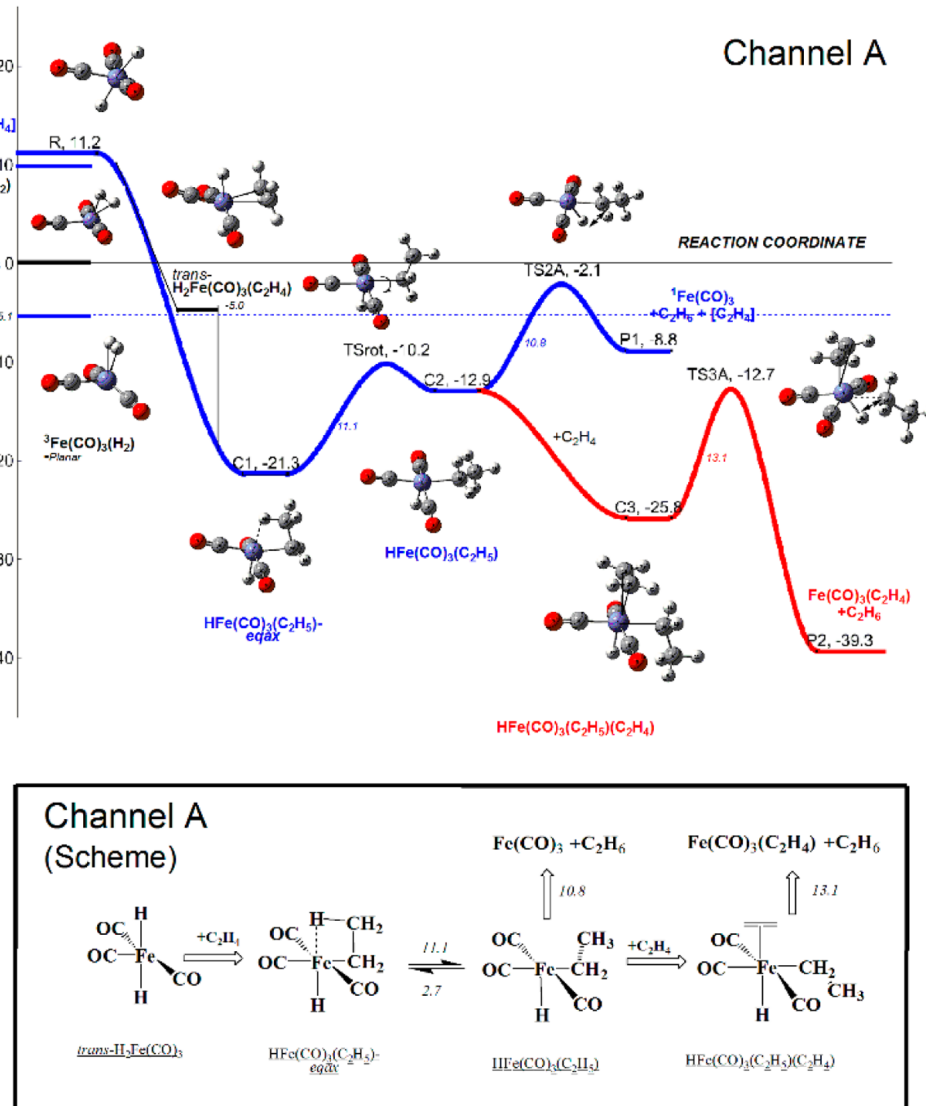


Figure 2. PES cross-section corresponding to ethylene hydrogenation assisted by *trans*-dihydridotricarbonyliron (channel A), calculated at B3LYP/LanL2DZ[Fe]/6-311+G(2d,p) [$\text{C}_2\text{H}_4\text{O}$] level. R, C1, C2, C3, P1, and P2 stand for reagent, intermediate complexes, and products, which are represented also by their chemical formulas and structures.

Consequently, the rate-determining step can vary depending on the details of the symmetry-specific elementary processes. Chemical and photochemical activation phenomena can play a decisive role in the branching ratios, given that the deactivation of metallocomplexes follows the same rules as those for simple organic counterparts, best described by RRKM and Quantum RRK theories (see, e.g., refs 54–57). Notably, highly vibrationally excited adducts have been observed in the photolysis of $\text{Fe}(\text{CO})_5$ and the carbonyls of other transition metals.⁵⁹

Detailed analyses of the reaction profiles are presented in the next subsections, followed by the summary of the PES results.

3.1. Reaction Channel A. Figure 1 presents the initial singlet and triplet spin-state bare structures of *trans*- $\text{H}_2\text{Fe}(\text{CO})_3$ reagent, ethylene-ligated species, as well as their early transformation products. The singlet-state *trans*- $\text{H}_2\text{Fe}(\text{CO})_3$ is the least stable isomer among the three dihydrides and is composed of two trans-oriented H-centers normal to the planar fragment of $\text{Fe}(\text{CO})_3$, in a quadratic pyramidal polyhedron. It has an energy ca. 11.2 kcal mol⁻¹ higher than the *cis*-dihydride.

The latter structure, in turn, is more stable than the *gauche*- $\text{H}_2\text{Fe}(\text{CO})_3$, by 6.6 kcal mol⁻¹. The energy of the most stable *cis*-isomer was selected as the origin (zero energy level) for all PES cross sections. Note that the global minimum of the PES of $[\text{H}_2\text{Fe}(\text{CO})_3]$ is the triplet dihydrogen nonclassical complex (vide infra). Two triplet isomers located at -4.9 and -5.1 kcal mol⁻¹ below the zero level, respectively, have been identified with different $\text{Fe}(\text{CO})_3$ core configurations (see also Figures 3 and 5 and Table 1).

The association between ethylene and the singlet spin-state *trans*-dihydridotricarbonyliron generates the singlet ethyl hydride adduct, $\text{HFe}(\text{CO})_3(\text{C}_2\text{H}_5)$, which subsequently converts to a higher energy isomer (a necessary step to produce ethane, as illustrated in Figure 2). It is interesting to note that the tricarbonyliron fragments of all species maintain the planar structure along the entire reaction coordinate (also for channel B, vide infra), involving pathways through the TS2A and TS3A transition states of the direct and bimolecular ethane-elimination reactions, respectively.

The association of dihydrides with ethylene typically forms a π -adduct (cf. Figures 4, 6, and 7) when the corresponding PES minimum is not too shallow and the π -complex is both thermodynamically and kinetically stable. The PES A constitutes an exception compared to the other channels (B, C, and D), because the reaction starts with a spontaneous rearrangement of the π -dihydride adduct, $H_2Fe(CO)_3(\eta^2-C_2H_4)$ to its ethyl hydride tautomer, $HFe(CO)_3(C_2H_5)$. Such a spontaneous hydride migration to the olefin and formation of a σ -complex occurs when the ethylene attacks the dihydride parallel to the H–Fe–H axis, which represents the diagonal of the basal plane of the corresponding quadratic iron-pyramidal polyhedron (Figure 1).

The monohydride adduct $HFe(CO)_3(C_2H_5)$ -eqax has a local octahedral structure and is additionally stabilized by an M–H–C agostic bond between a terminal H of the ethyl group and the metal center (Figures 1 and 2). The ethyl group is coordinatively bound to the equatorial (pseudoequatorial) position of the iron octahedron, whereas the agostic bond occupies the open axial position (denoted as eqax). Several agostic structures are involved in the other channels as well. Therefore, for the generality of notations, the only hydridic H of these complexes will be considered to be located at the axial position of the iron-octahedron.

The other three PES cross sections (B, C, and D), which are examined in the following sections, involve the formation of additional π -adducts through TS1i transition states, followed by hydride-migration reactions.

A higher energy isomer, *trans*- $H_2Fe(CO)_3(\eta^2-C_2H_4)$ dihydride, was also identified, in which ethylene is rotated 90° about the metal–ligand axis of the *trans*- $H_2Fe(CO)_3$; see Figure 1. It is located only at $-5.0\text{ kcal mol}^{-1}$ below the basic energy level of PES (the sum of energies of *cis*- $H_2Fe(CO)_3$ and C_2H_4). Due to the low energy barrier (ca. 1.2 kcal mol^{-1}), the rotation of the ligated ethylene group also generates the same eqax-ethyl monohydride adduct (pathway described at the bottom of Figure 1).

Figure 2 provides the elementary processes leading to ethane production in some detail (see also Table 2). As seen, an interconversion barrier TS_{rotA} of $11.1\text{ kcal mol}^{-1}$ height for the internal rotation of the ethyl fragment, which is necessary for hydrogenation to occur, is present.

The high barrier is a result of the high-stability of the agostic-ligated ethyl monohydride, because an additional energy is required for the scission of the agostic bonds and to allow intramolecular rearrangements.

The high energy ethyl monohydride isomer undergoes two alternative product formation processes: (i) a monomolecular C_2H_6 elimination via TS2A and (ii) a second-ethylene-assisted bimolecular reaction via TS3A. It is noteworthy that the barrier height of $10.8\text{ kcal mol}^{-1}$ for TS2A is still below that of the entrance channel, and even below the zero-level of the *cis*-dihydride isomer. The TS3A barrier has even lower energy. Consequently, both product formation reactions are accessible energetically provided that the processes start from any of the original dihydrides. The chemical (photochemical) activation generates an energized adduct able to overcome the barriers.

Direct (monomolecular) product formation pathway via TS2A regenerates the singlet-state bare tricarbonyliron, $Fe(CO)_3$, which can restart a new catalytic cycle (or undergo intersystem crossing to form its triplet counterpart). Similarly, the second ethylene-assisted process generates a singlet monohydride intermediate, $HFe(CO)_3(C_2H_5)(\eta^2-C_2H_4)$, fol-

lowed by the reductive elimination of ethane via TS3A. This process generates a π -complex $Fe(CO)_3(\eta^2-C_2H_4)$, which also serves as a catalyst-precursor. The subsequent reaction of $Fe(CO)_3(\eta^2-C_2H_4)$ with H_2 regenerates the catalytic cycle. As noted in the Introduction, such a 16-electron species has been identified in the photochemical experiments with $Fe(CO)_5$.¹ It has been suggested that it forms also via the loss of CO upon irradiation of $Fe(CO)_4(\eta^2-C_2H_4)$ matrices at low temperatures.^{36,41} In the gas phase it has been observed by Onda et al.⁵⁹

The well-depth for the first-ethylene association reaction is ca. 21 kcal mol^{-1} , which is close to those observed from the other PES cross sections (B, C, and D depicted in Figures 4 and 6), even though there are significant differences in the relative energies of the initial reagents. Perhaps channel A is active only when a downhill reaction occurs from the *trans*-dihydride. The ethylene combination with the other singlet-state reagents also allows gaining the internal “chemical activation” energy. Thus, an energized adduct will be capable of overcoming the higher TS2A barrier located significantly below the entrance channel ($13.3\text{ kcal mol}^{-1}$; 2.1 kcal mol^{-1} from the zero-level). On the other hand, the combination of a shallow rotamer minimum with the low isomerization barrier that precedes the TS2A and TS3A transition states, does not provide the adduct stabilization to allow the subsequent association of a second ethylene molecule. Thus, if channel A is active, it would most likely follow the monomolecular pathway mainly because of the presence of the high rotation barrier (TS_{rotA} of $11.1\text{ kcal mol}^{-1}$ height, Figure 2), and the small reverse barrier of the isomerization (2.8 kcal mol^{-1}), which prevent the stabilization of the intermediate necessary for the second pathway.

As indicated above, the triplet-state η^2 - $H_2Fe(CO)_3$ complex is the most stable configuration among all hydrogenated tricarbonylirons, yet its involvement is not sterically obvious for channel A. Instead, the triplet-state *trans*-dihydride is expected to provide the same products via the intersystem crossing via its singlet counterpart. According to DFT results, this isomer is located significantly higher in energy than its singlet counterpart, whereas the CCSD(T) single-point calculations (vide infra) predict a higher stability of the triplet dihydride (Table 1). Such a result is surprising for DFT because it is known that the B3LYP functional typically overestimates the stability of the higher spin states.^{68,74,75} Interestingly, the basis set extension on light atoms increases the stability of triplet *trans*- $H_2Fe(CO)_3$ at B3LYP level, whereas the BP86 functional using the same basis set predicts even much higher instability of triplet dihydride (Table 1). The all-electron B3LYP/6-311+G(2d,p) method also predicts close energies for the two isomers (the triplet isomer is more stable by about 0.5 kcal mol^{-1}). Overall, it is expected both trans-isomers to be generated in a specific photochemical condition.

Assuming that channel A is alternatively initiated by the spin-crossing between the original singlet PES and the triplet PES involving the triplet H_2 complex (located ca. 5 kcal mol^{-1} below the reference level of the *cis*- $H_2Fe(CO)_3 + C_2H_4$), the other processes that may occur become energetically more demanding. As shown by Figure 2, the transition-state TS_{rotA} is located below such an entrance level and therefore can occur energetically. The second ethylene-addition pathway is also possible because it has a lower energy by 7.6 kcal mol^{-1} , in contrast to the monomolecular reaction via transition-state TS2A which lies much higher in energy. Consequently, the direct ethane production is expected to be very slow. It will

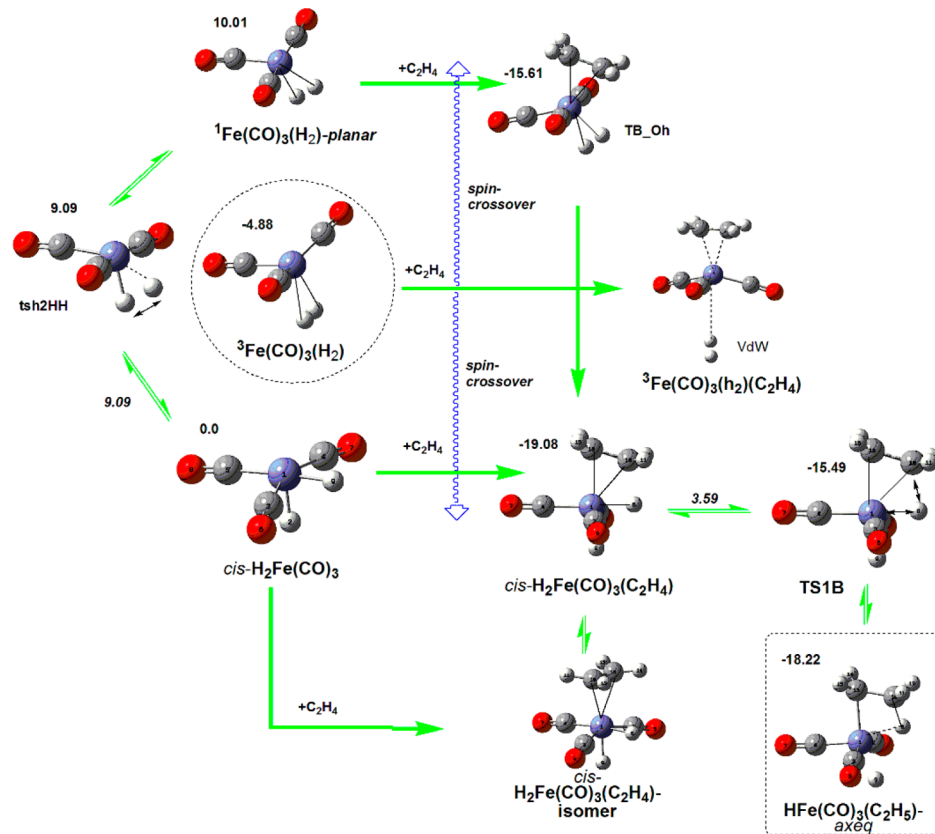


Figure 3. Initial steps involved in channel B. The numbers above the structures (in kcal mol^{-1}) indicate the stabilities relative to the *cis*-isomer, whereas the barrier heights are noted on the arrows. An ethyl hydride intermediate and a triplet $\text{Fe}(\text{CO})_3(\text{H}_2)$ reagent are outlined.

become even slower when the limited efficiency of the spin-crossing through a minimal energy crossing point (MECP)⁶⁵ is considered (see also the discussion below regarding the PES cross sections C and D). The effectiveness of the bimolecular second-ethylene-addition/ C_2H_6 -elimination pathway via TS3A is controlled by the rate-limiting barrier TS_{rotA} for the internal rotation of the ethyl group, which precedes the TS3A being located by 2.6 kcal mol^{-1} above that transition state.

Channel A, and the other three as well, involve processes related to the second H-transfer, viz., the formation of $\text{Fe}(\text{CO})_3(\text{C}_2\text{H}_5)_2$ isomeric complexes from corresponding π -intermediates $\text{HFe}(\text{CO})_3(\text{C}_2\text{H}_5)(\eta^2\text{-C}_2\text{H}_4)$.

3.2. Reaction Channel B. This channel is generated via the ethylene addition to the *cis*- $\text{H}_2\text{Fe}(\text{CO})_3$, where the H-ligands are located orthogonal to each other in the axial and equatorial positions of the quadratic pyramidal iron-polyhedron. The structural unit involving the three CO groups is located in the basal plane (Figure 3).

As noted above, the *cis*- $\text{H}_2\text{Fe}(\text{CO})_3$ is the most stable isomer among the three tricarbonyl dihydrides and its energy is considered as a reference energy level for all PESs. However, it has an energy higher by 4.9 kcal mol^{-1} (5.1 kcal mol^{-1} for the isomer involving the planar $\text{Fe}(\text{CO})_3$ core) compared to the most stable triplet dihydrogen complex ${}^3\text{Fe}(\text{CO})_3(\text{H}_2)$. Harvey and co-workers predicted an energy lower by 1.4 kcal mol^{-1} at the B3PW91* level,⁴⁹ in agreement with our GGA calculations at the BP86/LanL2DZ/6-311+G(2d,p) level, which also predicts a higher stability of the *cis*-dihydride complex ($-4.3 \text{ kcal mol}^{-1}$ for the planar configuration of the three CO groups and $-5.0 \text{ kcal mol}^{-1}$ for the angular configuration). However, our more refined CCSD(T) calculations based on the B3LYP

geometries predict a higher stability of the triplet dihydride by about 6.0 kcal mol^{-1} (Table 1). Following the PES cross-section A, the *cis*- $\text{H}_2\text{Fe}(\text{CO})_3$ reagent coordinates a bidentate ethylene ligand at the entrance channel (Figure 4 and Table 3) thus forming a *cis*- $\text{H}_2\text{Fe}(\text{CO})_3(\eta^2\text{-C}_2\text{H}_4)$ adduct with a well depth of 19.1 kcal mol^{-1} .

The adduct undergoes a rapid rearrangement via a small TS1B isomerization barrier height of 3.6 kcal mol^{-1} to generate ethyl monohydride $\text{HFe}(\text{CO})_3(\text{C}_2\text{H}_5)\text{-}axeq$ (the ethyl group is coordinatively bound to the axial position, whereas the agostic bond is directed to the equatorial position, designated as *axeq*). The low barrier is consistent with the experimental results of Weitz and co-workers, suggesting for the isomerization barriers of propane and pentane $<3.5 \text{ kcal mol}^{-1}$ and $<5.4 \text{ kcal mol}^{-1}$ values, respectively.³³

Figure 4 also displays the two elementary pathways to produce ethane (via the transition states TS2B and TS3B) analogous to those emphasized for channel A (Figure 2). The planar tricarbonyl core of the species involved in this PES cross-section remains almost undistorted. Channel B can also be generated through the association reaction of ethylene with the singlet dihydrogen complex $\text{Fe}(\text{CO})_3(\text{H}_2)$ to form a trigonal bipyramidal π -complex (TB_Oh), as illustrated in Figures 3 and 4, which spontaneously converts to the *cis*-dihydride. The same adduct can be formed by the intersystem crossing of the original PES with the triplet surface of the dihydrogen complex. Such a scenario is consonant with the novel ligand-addition mechanism of spin-forbidden reactions suggested by Besora et al. on the basis of the analysis of MECP obtained at B3PW91* DFT level.⁴⁹ Spin-crossover has been suggested to occur first, followed by ligand addition.

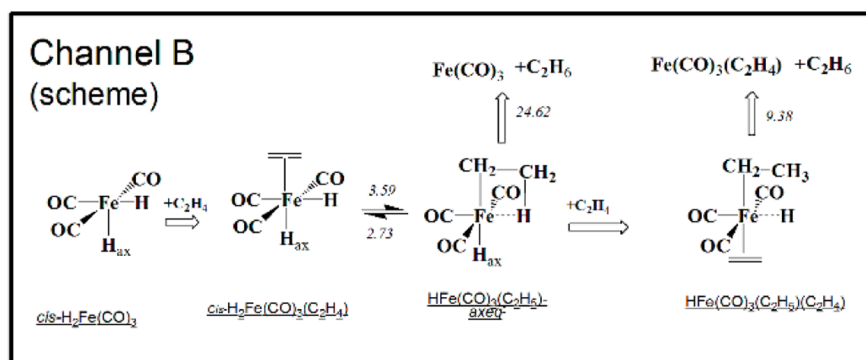
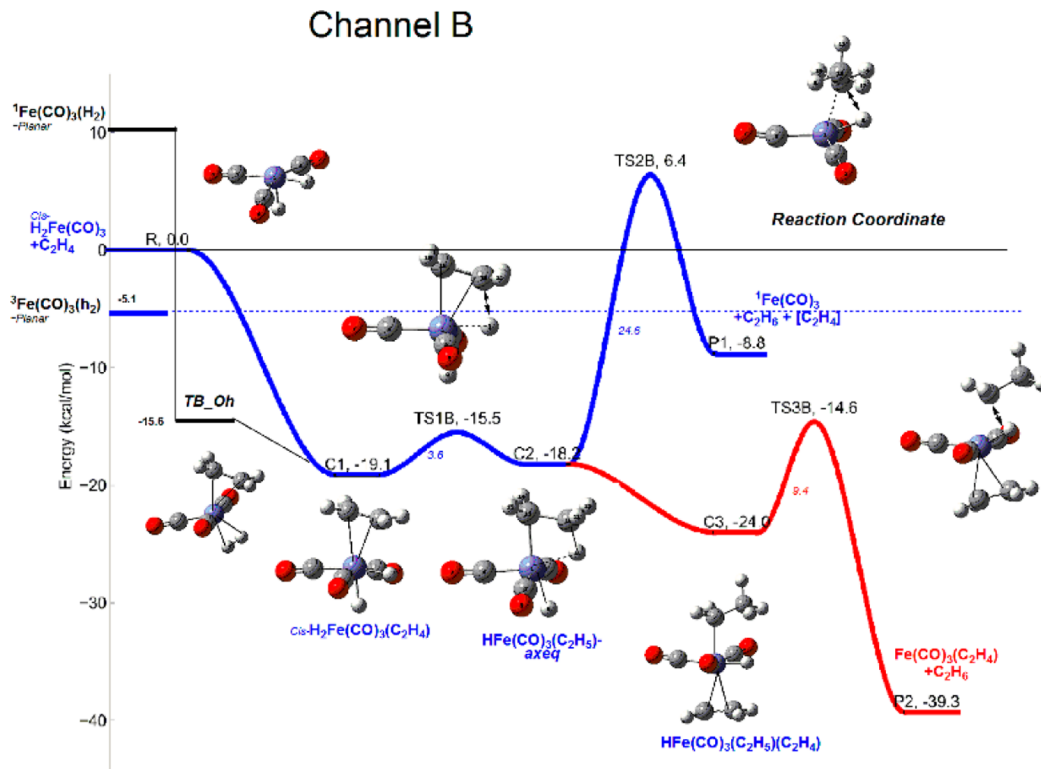


Figure 4. PES cross-section of ethylene hydrogenation assisted by *cis*-dihydridotricarbonyliron (channel B), calculated at B3LYP/LanL2DZ[Fe]/6-311+G(2d,p) [C,H,O] level where R, C1, C2, C3, P1, and P2 stand for reagent, intermediate complexes, and products, explicitly described by formulas and structures.

The ethyl group coordinatively bound to the metal center of the newly formed ethyl monohydride isomer $\text{HFe}(\text{CO})_3(\text{C}_2\text{H}_5)$ again plays the role of a bidentate ligand involving the agostic M–H–C bond between a H-atom of the terminal methyl group and the iron center. The geometry of $\text{HFe}(\text{CO})_3(\text{C}_2\text{H}_5)$ can be best described as a truncated octahedron bearing an “agostic H-ligand” in the vacant equatorial position (Figure 3).

Because of the additional stabilization of the ethyl-hydridotricarbonyl σ -complex, the passage of the “agostic-ligated” complex through the TS2B barrier becomes prohibitively high. This monomolecular reaction barrier for the direct C_2H_6 elimination is as large as 24.6 kcal mol⁻¹. Notably, it is the highest barrier among all analogous TS2i ones (cf. Figures 2, 4, and 6). It is located above the level of the entrance channel of

PES B by 6.4 kcal mol⁻¹. Consequently, an energized adduct has a too low probability to overcome this barrier.

Agostic bonds are common in organometallic chemistry.⁸⁷⁻⁸⁹ They have been also inferred by Harris and co-workers⁸⁹ to explain alkene isomerization by activated $\text{Fe}(\text{CO})_5$. They assumed that the triplet structure of the intermediate does not form an agostic bond, in contrast to the singlet species, perhaps because the coordinatively unsaturated metal center does not interact favorably with the saturated C–H bonds in the triplet state. They found that M–H–C agostic interaction is stabilized by more than 8 kcal mol⁻¹, the value close to what we found (vide infra).

Once the agostic-ligated *axeq*-ethyl hydride is formed and a second ethylene reacts, the system follows a downhill passage through a low-energy barrier TS3B to eliminate ethane. The energies of TS3B and TS1B are fairly close. Therefore, the

Table 3. Relative Energies (ΔE) and Enthalpies (ΔH) of Stationary Points along PES Cross-Section B^a (Channel B), in kcal mol⁻¹

species	ΔE	$\Delta H(298K)$
Fe(CO) ₃ (H ₂) + 2C ₂ H ₄	10.01	10.28
cis-H ₂ Fe(CO) ₃ + 2C ₂ H ₄	0.0	0.0
TB_Oh + C ₂ H ₄	-15.61	-16.25
³ Fe(CO) ₃ (H ₂) + 2C ₂ H ₄	-5.07	-4.17
cis-H ₂ Fe(CO) ₃ (η^2 -C ₂ H ₄) + C ₂ H ₄	-19.08	-19.73
TS1B + 2C ₂ H ₄	-15.49	-16.48
HFe(CO) ₃ C ₂ H ₅ -eqax + C ₂ H ₄	-18.22	-19.07
TS2B + C ₂ H ₄	6.40	6.16
Fe(CO) ₃ + C ₂ H ₆ + C ₂ H ₄	-8.83	-8.75
³ Fe(CO) ₃ + C ₂ H ₆ + C ₂ H ₄	-29.10	-29.22
HFe(CO) ₃ (C ₂ H ₅)(η^2 -C ₂ H ₄)	-24.01	-25.13
HFe(CO) ₃ (C ₂ H ₅) ₂ -axeq2B	-25.52	-25.73
TS3B	-14.63	-15.61
Fe(CO) ₃ (η^2 -C ₂ H ₄) + C ₂ H ₆	-39.26	-39.78
³ Fe(CO) ₃ (η^2 -C ₂ H ₄) + C ₂ H ₆	-47.61	-47.41

^aAll energies are relative to *cis*-dihydride isomer, cis-H₂Fe(CO)₃ + 2C₂H₄ calculated at B3LYP/LanL2DZ[Fe]/6-311+G(2d,p) [C,H,O] level. Zero-point vibration energies are included.

isomerization barrier limits the rate of the bimolecular reaction that follows.

The direct product formation via TS2B is unlikely to occur at low temperatures. The high forward barrier for the monomolecular decomposition of the axeq structure, combined with the relatively fast equilibrium with the π -adduct, kinetically stabilizes the ethyl monohydride complex, to allow the coordination of a second C₂H₄ molecule. This increases the probability of the bimolecular gas-phase reaction, unlike what occurs in channel A. When the process is triggered by the *cis*-dihydride isomer (with a well-depth of the association reaction with ethylene being 19.1 kcal mol⁻¹), the energized gas-phase adduct can be readily overcome both TS1B and TS3B barriers, increasing the likelihood of the bimolecular process via TS3B.

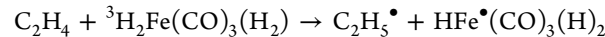
The intersystem crossing of ³Fe(CO)₃(H₂) triplet-dihydrogen-complex-initiated pathway can occur with either its singlet counterpart or the *cis*-dihydride-generated pathway, followed by the course of the original singlet PES. As shown by Figure 4, the second ethylene-addition pathway via TS3B becomes possible being located below (by 9.5 kcal mol⁻¹) the triplet entrance energy level. In contrary, the transition-state TS2B for the monomolecular reaction lies significantly higher in energy. On the other hand, the low isomerization barrier via TS1B will also be accessible energetically.

It should be also noted that the singlet HFe(CO)₃(C₂H₅)-axeq intermediate can form its triplet counterpart via a vertical excitation energy of 15.9 kcal mol⁻¹ followed by the generation of ³Fe(CO)₃ through a straightforward ³TS2B barrier of activation (ca. 6 kcal mol⁻¹). This triplet barrier is somewhat lower than the corresponding singlet barrier TS2B (by 2.4 kcal mol⁻¹).

Generally, the two unpaired electrons in both the triplet dihydrogen and the ethylene π -complexes are located on the Fe atoms. Similarly, the corresponding spin density in the monohydride HFe(CO)₃(C₂H₅) reagent of the above process is mostly localized on the iron center ($\rho_{Fe} = 1.81e$). However, it is significantly reduced for the transition-state ³TS2B ($\rho_{Fe} = 1.36e$). The unpaired electron is partly shifted to the proximal carbon atom of the newly formed C₂H₆ ($\rho_C = 0.35e$). In

contrast to the H-abstraction reactions with radicals, where the final spin transfer generates a new radical, the unpaired electron in the triplet reaction is transferred back to the Fe center to form triplet ³Fe(CO)₃ and the singlet C₂H₆ products, as demonstrated by additional calculations for the selected intermediates along the reaction coordinate.

On the other hand, the distribution of spin density along the reaction coordinate in the direct triplet H-abstraction reactions such as



is similar to that in the conventional radical reactions, viz., one of the unpaired electrons in the TS is shared by the transferring-H and the hydrogen donor-Fe centers (the second electron remains located on the Fe atom), and the final spin transfer generates two radical species, as shown in the above reaction scheme. This reaction was not considered further because of the high activation barrier.

3.3. Reaction Channels C and D. Both reaction channels originate from ethylene coordination with the same *gauche*-H₂Fe(CO)₃ dihydride reagent to form a metastable *gauche*-H₂Fe(CO)₃(η^2 -C₂H₄) adduct (Figures 5–7 and Tables 4 and 5). Unlike the other two dihydrides (*cis* and *trans*) involved in channels A and B, respectively, the *gauche* isomer bears an angular tricarbonyliron core Fe(CO)₃ consisting of three nearly orthogonal to each other Fe–CO bonds, which remains unchanged during the processes involved in channels C and D.

Figure 5 displays the early transformations triggered by the *gauche*-H₂Fe(CO)₃ reagent, starting with its dihydride–dihydrogen isomerization and the processes that follow its complexation with ethylene. As shown on the left-hand side of Figure 5, the dihydrogen complex–dihydride conversion via transition-state TSh2HH can easily occur prior to the π -complexation of systems involving the angular Fe(CO)₃ core. The forward reaction barrier leading to the *gauche*-H₂Fe(CO)₃ dihydride is 2.3 kcal mol⁻¹, whereas for the reverse reaction it is 3.0 kcal mol⁻¹. Notably, the BP86 GGA calculations predict the barrier 3.2 kcal mol⁻¹ (the reverse barrier being 4.0 kcal mol⁻¹), which is only somewhat higher than the barrier calculated at the hybrid B3LYP level using the same basis set.

It is noteworthy that the analogous barrier transforming the planar configuration of *cis*-H₂Fe(CO)₃ to dihydrogen complex is as high as 9.1 kcal mol⁻¹ (“late transition state”), whereas the reverse reaction is nearly barrierless (Figure 3). A barrier for the dihydrogen complex–dihydride conversion of 10.6 kcal mol⁻¹ was also calculated by Besora et al. using the B3PW91* method, which involved a reduced (to 10%) contribution of the exact exchange-HF potential.⁴⁹

The initial portion of the PES shared by C and D channels is fairly complex (Figure 5–7). It involves several interconversion processes between numerous nearly identical structures with close energies. In addition to the stereoisomers presented in Figure 5, two types of rotamers involved in the formation of *gauche*-H₂Fe(CO)₃(η^2 -C₂H₄) dihydridic π -complex were also identified not presented here for the sake of simplicity.

Dihydridic *gauche*-H₂Fe(CO)₃(η^2 -C₂H₄) adduct undergoes isomerization via the H-transfer to the ethylene moiety through the TS1C/D barrier of about 5 kcal mol⁻¹ to form the more stable ethyl monohydridotricarbonyliron σ -complex.

It should be noted that none of the applied methods could locate the two stationary points simultaneously. The calculations were converging to either the TS1C/D transition-state

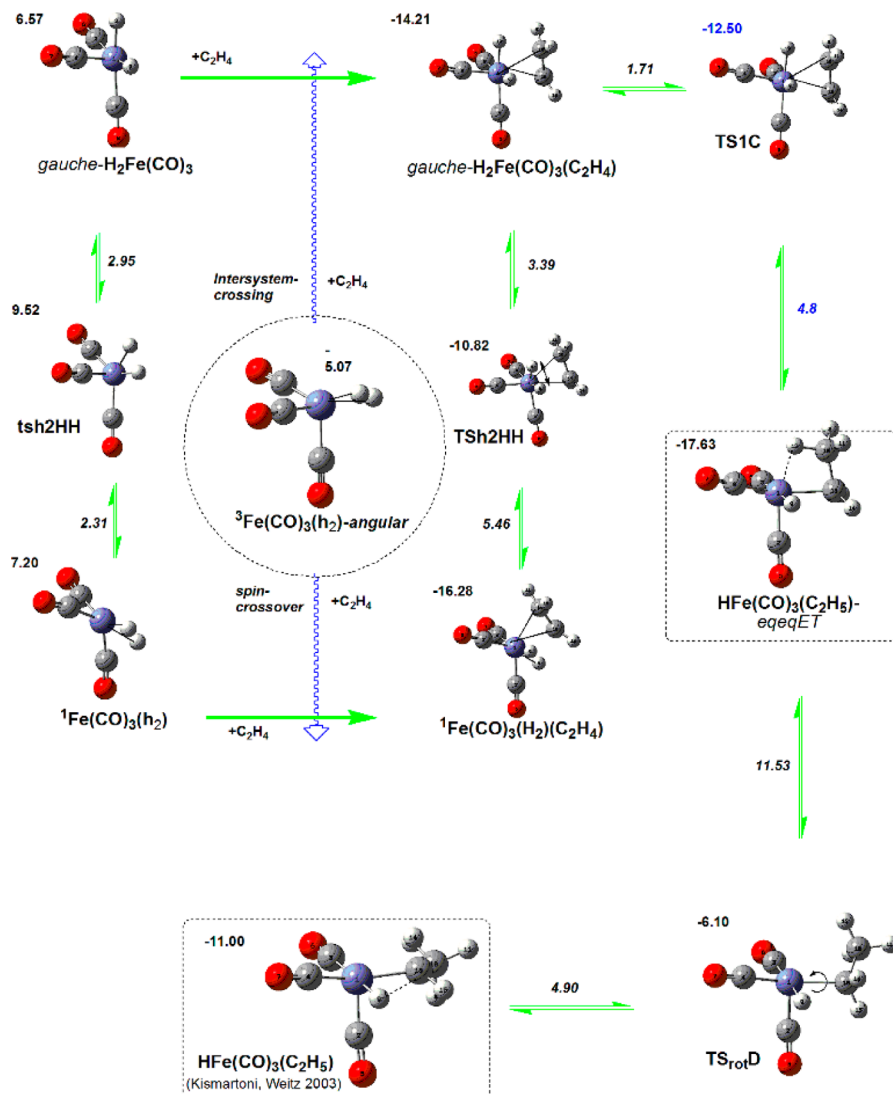


Figure 5. Initial steps involved in channels C (the top part) and D (the bottom line). All species maintain an angular Fe(CO)₃ structural motif. The numbers above the structures (in kcal mol⁻¹) provide the stabilities relative to the cis-isomer, whereas the barrier heights are indicated on the arrows. Two ethyl-hydrido intermediates and a triplet Fe(CO)₃(H₂) reagent are outlined.

or gauche-hydridic compound or to another stationary point of Figure 5, such as the monohydride.

The forward reaction barrier indicated above was evaluated from the reverse barrier of 8.5 kcal mol⁻¹ calculated at the single-point B3LYP/LanL2DZ/6-311+G(2d,p)//BP86/LanL2DZ/6-311+G(2d,p) level. This reverse barrier height is in agreement with full optimization results on the levels of BP86/LanL2DZ/6-311+G(2d,p), BP86/LanL2DZ, BP86/sdd, and B3PW91/sdd, which provide the values 9.2, 9.1, 8.1, and 10.1 kcal mol⁻¹, respectively. The energy difference between the gauche and the eqeq intermediates of 3.4 kcal mol⁻¹ was then subtracted from the reverse barrier of 8.5 kcal mol⁻¹.

The *gauche*-H₂Fe(CO)₃(η^2 -C₂H₄) is represented by a minimum along the energy descent curve that transforms this compound into the HFe(CO)₃(C₂H₄)-*eqeq* intermediate. Its structure is almost identical to that of TS1C. The methods that locate the transition state, e.g., BP86 and B3PW91 in conjunction with LanL2DZ standard basis set, fail to locate a minimum (the reagent) in contrast to the all-electron BP86 and B3PW91 methods, as well as the B3LYP method using various basis sets. The low TS1C/D barrier obtained agrees with the

experimentally based conclusions of Wells and Weitz that the conversion of Fe(CO)₃(H₂)C₂H₄ is not rate limiting for the entire process.³³ It is also consonant with other experimental data of Weitz and co-workers concerning the isomerization of propane and pentane the barrier heights of which are <3.5 and <5.4 kcal mol⁻¹, respectively.³⁷

The “global” adduct HFe(CO)₃C₂H₅-*eqeq* is also stabilized by an M–H–C agostic bond between Fe and the β -H of the ethyl moiety. Both ethyl group bonding features are located in equatorial (pseudoequatorial³⁸) positions bound either coordinatively or agistically to the equatorial position of the metal octahedron (Figures 5 and 6), the reason for which the *eqeq* suffix is chosen (the position of the hydridic H is considered as the axial position, as also specified above). The structure of the HFe(CO)₃(C₂H₅)-*eqeq* complex can be described as that of a distorted truncated octahedron bearing an “agostic H-ligand” on the open site, which is located on the equatorial position. The agostic interaction additionally stabilizes the σ -complex by about 8 kcal mol⁻¹ (vide infra).

The HFe(CO)₃(C₂H₅)-*eqeq* intermediate generates two distinct product formation channels, C and D, as illustrated

Table 4. Relative Energies (ΔE) and Enthalpies (ΔH) of Stationary Points along PES Cross-Section C^a (Channel C), in kcal mol⁻¹

species	ΔE	$\Delta H(298K)$
gauche-H ₂ Fe(CO) ₃ + 2C ₂ H ₄	6.57	6.65
Fe(CO) ₃ (H ₂) + 2C ₂ H ₄	7.20	7.81
cis-H ₂ Fe(CO) ₃ + 2C ₂ H ₄	0.0	0.0
³ Fe(CO) ₃ (H ₂) + 2C ₂ H ₄	-4.88	-3.78
Fe(CO) ₃ (H ₂)(η^2 -C ₂ H ₄) + C ₂ H ₄	-16.28	-16.88
TSh2HH + C ₂ H ₄	-10.82	-10.60
gauche-H ₂ Fe(CO) ₃ (η^2 -C ₂ H ₄) + C ₂ H ₄	-14.21	-14.88
TS1C/D + C ₂ H ₄	-9.11 ^b	-9.55 ^b
HFe(CO) ₃ C ₂ H ₅ -eqeq + C ₂ H ₄	-17.63	-18.57
TS2C + C ₂ H ₄	-7.15	-8.05
Fe(CO) ₃ + C ₂ H ₆ + C ₂ H ₄	-8.83	-8.75
³ Fe(CO) ₃ + C ₂ H ₆ + C ₂ H ₄	-29.10	-29.22
HFe(CO) ₃ (C ₂ H ₅)(η^2 -C ₂ H ₄)	-21.22	-22.50
HFe(CO) ₃ (C ₂ H ₅) ₂ -axeq2C	-29.85	-31.33
TS3C	-12.43	-14.00
Fe(CO) ₃ (η^2 -C ₂ H ₄) + C ₂ H ₆	-39.26	-39.78
³ Fe(CO) ₃ (η^2 -C ₂ H ₄) + C ₂ H ₆	-47.61	-47.41

^aAll energies are relative to *cis*-dihydride isomer, *cis*-H₂Fe(CO)₃ + 2C₂H₄ calculated at the B3LYP/LanL2DZ[Fe]/6-311+G(2d,p) [C₂H₆O] level. Zero-point vibration energies are included. ^bSee section 3.3 for explanations.

Table 5. Relative Energies (ΔE) and Enthalpies (ΔH) of Stationary Points along PES Cross-Section D^a (Channel D), in kcal mol⁻¹

species	ΔE	$\Delta H(298K)$
gauche-H ₂ Fe(CO) ₃ + 2C ₂ H ₄	6.57	6.65
Fe(CO) ₃ (H ₂) + 2C ₂ H ₄	7.20	7.81
cis-H ₂ Fe(CO) ₃ + 2C ₂ H ₄	0.0	0.0
³ Fe(CO) ₃ (H ₂) + 2C ₂ H ₄	-4.88	-3.78
Fe(CO) ₃ (H ₂)(η^2 -C ₂ H ₄) + C ₂ H ₄	-16.28	-16.88
TSh2HH + C ₂ H ₄	-10.82	-10.60
gauche-H ₂ Fe(CO) ₃ (η^2 -C ₂ H ₄) + C ₂ H ₄	-14.21	-14.88
TS1C/D + C ₂ H ₄	-9.11 ^b	-9.55 ^b
HFe(CO) ₃ C ₂ H ₅ -eqeq + C ₂ H ₄	-17.63	-18.57
TS _{rotD} + C ₂ H ₄	-6.10	-6.94
HFe(CO) ₃ C ₂ H ₅ -W + C ₂ H ₄	-11.00	-11.46
TS2D + C ₂ H ₄	-1.93	1.61
Fe(CO) ₃ + C ₂ H ₆ + C ₂ H ₄	-8.83	-8.75
³ Fe(CO) ₃ + C ₂ H ₆ + C ₂ H ₄	-29.10	-29.22
HFe(CO) ₃ (C ₂ H ₅)(η^2 -C ₂ H ₄)	^c	^c
HFe(CO) ₃ (C ₂ H ₅) ₂ -AxEq2D	-31.18	-32.58
TS3D	-13.13	-14.45
Fe(CO) ₃ (η^2 -C ₂ H ₄) + C ₂ H ₆	-39.26	-39.78
³ Fe(CO) ₃ (η^2 -C ₂ H ₄) + C ₂ H ₆	-47.61	-47.41

^aAll energies are relative to *cis*-dihydride isomer, *cis*-H₂Fe(CO)₃ + 2C₂H₄ calculated at the B3LYP/LanL2DZ[Fe]/6-311+G(2d,p) [C₂H₆O] level. Zero-point vibration energies are included. ^bSee section 3.3 for explanations. ^cConverges to the axeq2D global isomer.

in Figures 6 and 7, which involve two different sets of transition states, TS2C, TS3C and TS2D, TS3D, respectively, as channels A and B.

Channel D involves an isomer of the HFe(CO)₃(C₂H₅) complex identified theoretically by Weitz and co-workers⁵⁸ (hereafter referred to as the Weitz isomer, Figures 5–7). The comparison with our results shows a reasonable agreement in

structure and energy of this isomer. The Weitz isomer is located well above the products of the second olefin-addition reaction C₂H₆ + Fe(CO)₃(η^2 -C₂H₄) by 37.6 kcal mol⁻¹ vs 36.3 kcal mol⁻¹ at the BP86 level of Weitz et al.⁵⁸ On the other hand, this isomer is less stable than the *gauche*-dihydride intermediate by 5.28 kcal mol⁻¹, vs 10 kcal mol⁻¹ of Weitz et al. On the basis of thermochemical calculations, Weitz and co-workers concluded that the monomolecular product-formation process is most likely to occur. This is a significant conclusion, which is justified below at the level of calculated activation barriers and detailed examination of PES.

Our comprehensive analysis of the PES revealed that the monohydride isomer identified theoretically by Weitz et al.⁵⁸ have significantly higher energy than the several monohydride complexes identified by us (Figures 5–7). Therefore, the Weitz isomer can be hardly considered as the most relevant isomer for key mechanistic (kinetic) conclusions. Moreover, the high endothermicity of its formation (10 and 12 kcal mol⁻¹ at B3LYP and BP86 levels, respectively⁵⁸) would imply even higher kinetic barrier for its formation.

Indeed, our calculations revealed that a significant rotation barrier TS_{rotD} (11.5 kcal mol⁻¹) is required to form the Weitz isomer from the relevant HFe(CO)₃(C₂H₅)-eqeq monohydride. Channel D involves a TS2D barrier of 9.1 kcal mol⁻¹ to produce ethane via the monomolecular reductive-elimination pathway (Figure 7). The second ethylene assisted ethane formation channel via TS3D is also unfavored because of the same initial high rotation barrier TS_{rotD}. Consequently, both product formation pathways involved in this channel (via TS2D and TS3D) are less favored energetically. In addition, channel D does not provide for the bimolecular ethane elimination because of the low reverse barrier to the HFe(CO)₃(C₂H₅)-eqeq adduct (4.9 kcal mol⁻¹), which does not allow the intermediate to become sufficiently stabilized to acquire another ethylene molecule.

However, the general conclusion of Weitz and co-workers regarding the possibility of the monomolecular reaction is confirmed by our results based on the alternative, much-lower energy channel C described in Figure 6. A closer look at the PES revealed two new product formation pathways, via the monomolecular and bimolecular TS2C and TS3C transition states, respectively, which occur directly from the HFe(CO)₃(C₂H₅)-eqeq intermediate and avoid the supplementary barrier TS_{rotD} (Figure 6). The branching of the two C and D channels occurs once the agostic-ligated complex is obtained. Channel C provides the most efficient product formation pathways. The combined barrier for the direct product formation reaction via TS2C is 10.5 kcal mol⁻¹ (well below the entrance channel), against 20.6 kcal mol⁻¹ for the analogous process through channel D. The second-ethylene-addition reaction (TS3C) is also favored because its barrier is located 12.4 kcal mol⁻¹ below the reference energy level, and only 1.8 kcal mol⁻¹ above the *gauche*-H₂Fe(CO)₃(C₂H₄) adduct. In addition, the monohydride intermediate is more stable kinetically (cf. Figures 6 and 7).

3.4. Involvement of Dihydrogen Complexes and Triplet-State PES. As noted in the Introduction, the identification of the actual forms of the hydrogenated iron carbonyl complexes in the photochemical experiments with Fe(CO)₅ is very difficult and involves uncertainties. Different stereoisomers of dihydrides can be formed and contribute to the overall reaction. Therefore, all isomers (even the high energy ones) should be considered in the reaction schemes.

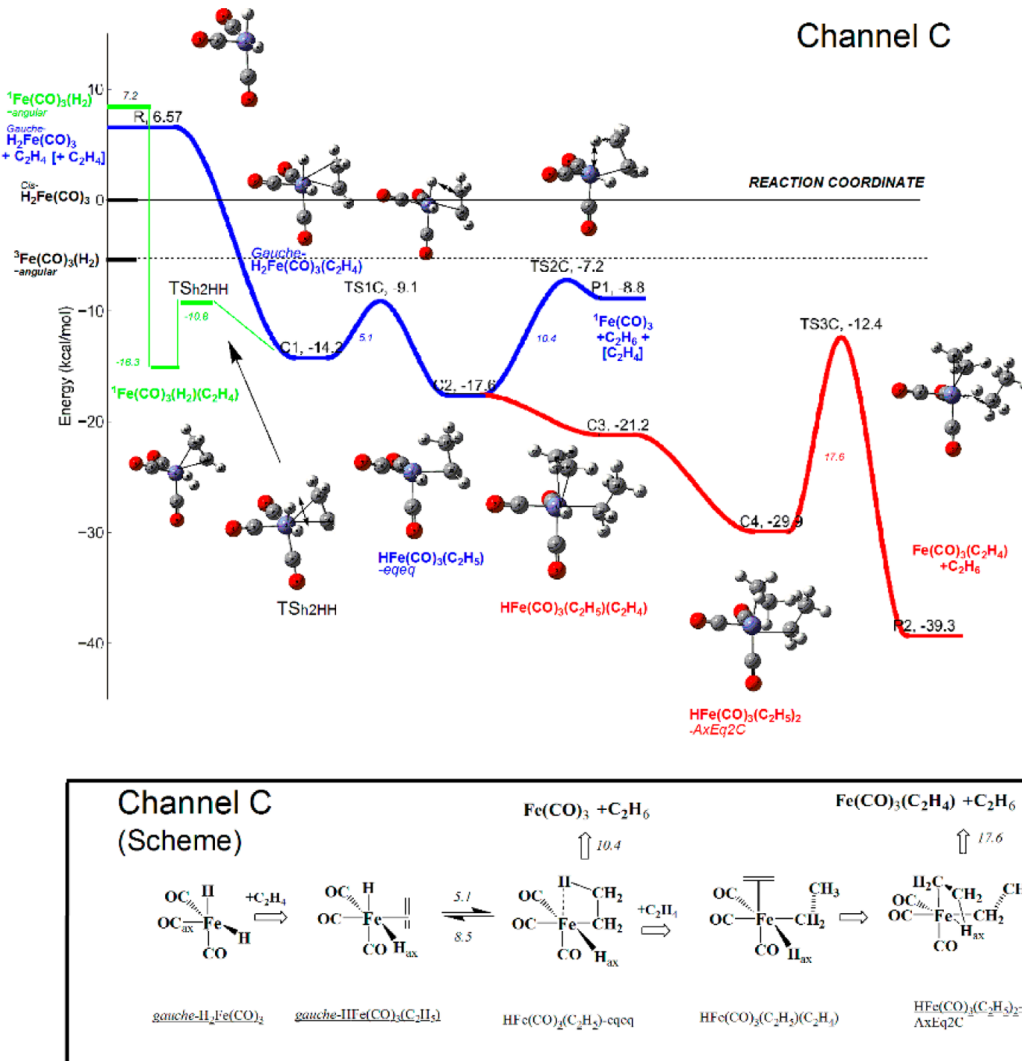


Figure 6. PES cross-section corresponding to ethylene hydrogenation assisted by *gauche*-dihydridotricarbonyliron (channel C) calculated at the B3LYP/LanL2DZ[Fe]/6-311+G(2d,p) [C₂H₆O] level. The pathway originated from the singlet H₂ complex is highlighted in green. R, C1, C2, C3, C4, P1, and P2 stand for reagent, intermediate complexes, and products.

According to Besora et al. using the B3PW91* DFT level of calculations, the *cis*-dihydride H₂Fe(CO)₃ isomer is the most stable isomer of the tricarbonyliron dehydrogenates,⁴⁹ as opposed to the results of Weitz and co-workers at the BP86 and B3LYP levels,⁵⁸ who found the triplet dihydron complex as the most stable one. Our more detailed B3LYP/LanL2DZ/6-311+G(2d,p) calculations combined with the high level calibrated results at CCSD(T) level revealed that the triplet dihydron, ³Fe(CO)₃(H₂), is the most stable isomer of the all hydrogenated tricarbonyliron complexes (Table 1). Two isomeric triplet structures of ³[η^2 -Fe(CO)₃(H₂)] containing nearly planar and angular Fe(CO)₃ structural motifs presented in Figures 3 and 5 and Tables 4 and 5 were particularly identified by us. The angular triplet isomer involved in Figure 5 was previously identified.^{49,58} Albeit two triplet isomers are almost isoenergetic, they differ structurally and serve as initial reagents to generate different reaction channels with different energy profiles.

An iron tricarbonyl hydrogenate intermediate has been detected in the photolysis of Fe(CO)₅ in supercritical *scr*Ar doped with H₂ by Besora et al. assigned to as a triplet dihydron complex, ³Fe(CO)₃(H₂).⁴⁹ On the basis of their

own calculations, they concluded that it cannot be a singlet Fe(CO)₃(H₂), because it then would decay more rapidly via a barrierless addition to CO than that observed experimentally. A minimal energy crossing point (MECP) connecting reagents to the singlet dihydron complex was identified at 6.6 kcal mol⁻¹ which was expected to provide a smaller rate constant for a triplet–singlet spin change. The detected intermediate was not considered a dihydron as well, as a MECP crossing point leading directly to a dihydron could not be identified, even though their calculations (*vide supra*) indicated a superior stability for the dihydron.⁹⁰

Consequently, alternative mechanisms for generation of reaction channels C and D by either singlet or triplet dihydron complexes should also be considered. This topic was in part examined in the previous sections concerning channels A and B, where a π -complex H₂Fe(CO)₃(η^2 -C₂H₄) (the catalyst) was generated via the ethylene ligation to the singlet-state η^2 -H₂Fe(CO)₃ complex bearing a planar tricarbonyliron fragment. A similar pathway in the initial portions of the both C and D PES cross sections was identified highlighted in green in Figures 6 and 7. The lower energy adduct η^2 -H₂Fe(CO)₃(η^2 -C₂H₄), formed from the singlet dihydron

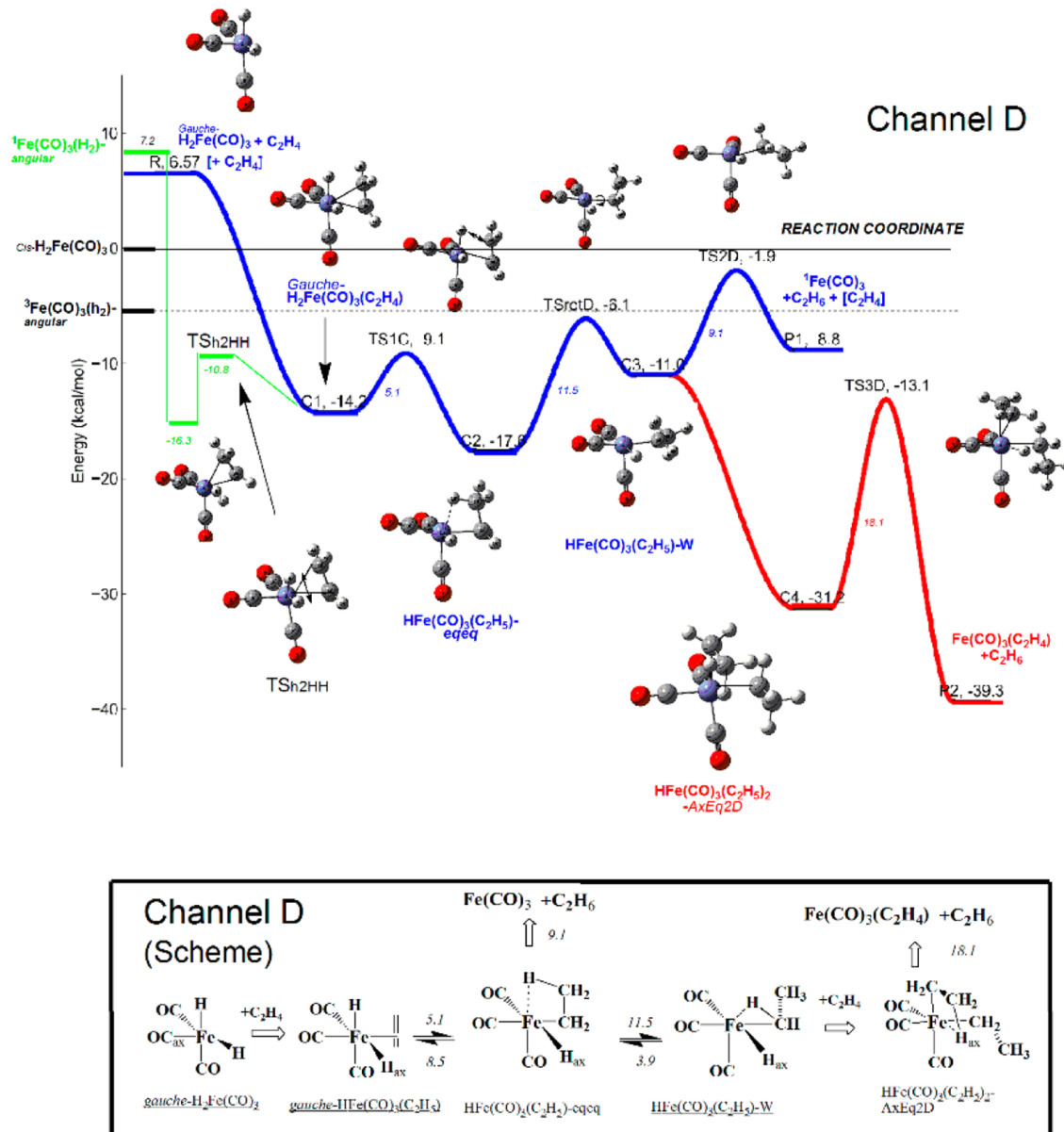


Figure 7. PES cross-section corresponding to the ethylene hydrogenation assisted by *gauche*-dihydridotricarbonyliron (channel D) calculated at the B3LYP/LanL2DZ[Fe]/6-311+G(2d,p) [C,H,O] level. The pathway originated from the singlet H_2 complex is highlighted in green. R, C1, C2, C3, P1, and P2 stand for reagent, intermediate complexes, and products.

complex bearing the angular $\text{Fe}(\text{CO})_3$ core, isomerizes into the dihydride π -complex, *gauche*- $\text{H}_2\text{Fe}(\text{CO})_3(\text{C}_2\text{H}_4)$, with a barrier height of 5.5 kcal mol⁻¹, merging into the original hydrogenation route.

In contrast to the singlet reactions, the triplet PES of the combined system is mostly repulsive. We have identified only a few triplet spin-state structures along channels C and D. The *gauche*- $\text{H}_2\text{Fe}(\text{CO})_3(\eta^2\text{-C}_2\text{H}_4)$ adduct (as well as its other isomers) is unstable in the triplet state for all identified singlet-state geometries and falls apart into the triplet H_2 complex $\text{Fe}(\text{CO})_3(\text{H}_2)$ and C_2H_4 (vide infra). The dihydride–dihydrogen conversion transition-state TSh2HH as well as other structures of singlet PES also do not converge to a proper minimum in the triplet states. The optimization of the triplet dihydrogen complex ${}^3\text{Fe}(\text{CO})_3(\text{H}_2)(\text{C}_2\text{H}_4)$ shows defragmentation. Notably, a transition-state search of the initial geometry of TS1C at the BP86/LanL2DZ level leads to

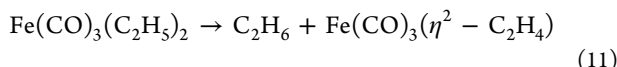
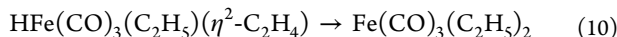
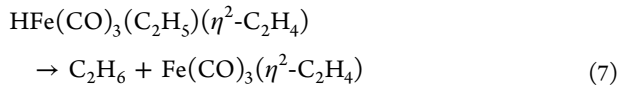
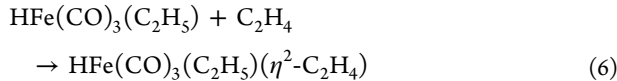
hydroformylation (one of the hydridic H-atoms is transferred rapidly to the proximal CO to form a formyl ligand, HCO).

Consequently, an intersystem crossing must occur either with its singlet counterpart or with the dihydride pathway, followed by the course of the original singlet PES when the process starts from an ethylene coordinated to the triplet $\text{Fe}(\text{CO})_3(\text{H}_2)$ complex. The singlet $\text{Fe}(\text{CO})_3(\text{H}_2)$ pathway then merges to the dihydride PES, as noted above. As shown in Figures 6 and 7, most identified transition states along channels C and D are located below the triplet entrance energy level and are therefore accessible energetically. Second ethylene-addition reaction can also occur. The corresponding TS3C and TS3D barriers are below the reference energy by 7.5 and 8.3 kcal mol⁻¹, respectively. The only transition-state TS2D for the monomolecular reaction lies high in energy unlike TS2C.⁷⁹ The transition-state TS1C is by 4.3 kcal mol⁻¹ below the energy of triplet reagent level, whereas the energies of the transition states

TS2C and TS3C leading to product formation, are lower in energy by 2.3 and 7.5 kcal mol⁻¹, respectively. As a result, even assuming that channel C is initiated by the triplet H₂ complex it would be still suitable for ethane formation (dependent on the efficiency of the intersystem crossing). Thus, channel C provides the *best scenario* for the hydrogenation of ethene by iron pentacarbonyl, providing that the reagents are energetically accessible!

On the other hand, the TS2D barrier not only is too high but also is combined with an additional rotation barrier to form the relevant reagent, the Weitz isomer. The rate of the bimolecular reaction is also controlled by the preceding rotation barrier, even though the TS3D transition state is located below the entrance channel by 8.3 kcal mol⁻¹. Consequently, the D-channel provides the least likely pathway to product formation. In addition, the Weitz isomer is consumed by forming the fairly stable dialkyl Fe(CO)₃(C₂H₅)₂ complex (*vide infra*).

3.5. Second-Ethylene Insertion Reaction (Second H-Transfer). The addition of the second ethylene molecule to the stabilized ethyl hydride intermediate HFe(CO)₃(C₂H₅) produces via eq 6 the π -complex HFe(CO)₃(C₂H₅)(η^2 -C₂H₄). Adduct thus formed undergoes a reductive elimination of ethane via reaction 7 mediated by TS3i. However, it can also isomerize via eq 10 to form the new σ -complex Fe(CO)₃(C₂H₅)₂, via another H-transfer reaction, analogous to the basic reaction 2. The Fe(CO)₃(C₂H₅)₂ complex constitutes the dialkyl analogue of tricarbonyliron dihydride H₂Fe(CO)₃. The subsequent reductive elimination of ethane occurs via the same TS3i transition state (eq 11), which is similar to the reaction 8 via TS2i.



These processes were not included in the PES profiles of channels A and B because they are sterically irrelevant for ethane production. Channel A simply does not have the opportunity to form Fe(CO)₃(C₂H₅)₂ σ -complex because the hydridic H-atom and the ethylene group are located at different sides of the Fe(CO)₃ plane (Figure 2). Instead, the second H-transfer within channel B forms a stable σ -complex, Fe(CO)₃(C₂H₅)₂-*axe*q2B, via a small barrier. However, no opportunity is seen for the ethane elimination here as well because two ethyl groups have opposite locations with respect to the Fe(CO)₃ plane (Figure 4). Therefore, the formation of Fe(CO)₃(C₂H₅)₂-*axe*q2B can be considered as a degenerative mechanism for the removal of the catalyst precursor Fe(CO)₃ from the reaction medium. According to experiment,^{32,33} the production of ethane was ended long before the feedstock of H₂ and C₂H₄ were consumed, suggesting the existence of a sink-mechanism, which waste the catalyst or its precursor. The formation of Fe(CO)₃(C₂H₅)₂-*axe*q2B coproduct provides a novel sink mechanism to explain experimental data.

In contrast to channels A and B, the above reactions can significantly alter the bimolecular reaction rates and overall

processes involved in channels C and D. The corresponding σ -complexes Fe(CO)₃(C₂H₅)₂-*axe*q2C and Fe(CO)₃(C₂H₅)₂-*axe*q2D are generated more easily (Figures 6 and 7). The complex Fe(CO)₃(C₂H₅)₂-*axe*q2D, which is formed via channel D, is somewhat more stable than its counterpart from channel C (by 1.3 kcal mol⁻¹).

3.6. Overview of PES Cross Sections. The overall results regarding the potential energy surfaces and identified reaction channels can be summarized as follows:

- (a) There are four separate reaction channels corresponding to the four cross sections (slices) of the PES of H₂Fe(CO)₃ + 2C₂H₄, denoted A, B, C, and D, at variance with the configuration of initial dihydridotricarbonyliron reagents (Figures 2, 4, 6, and 7).
- (b) Channels A and B are generated from the *trans*- and *cis*-H₂Fe(CO)₃ complexes, respectively, which contain a planar Fe(CO)₃ fragment (core) within a quadratic pyramidal or octahedral iron polyhedron. The tricarbonyliron core remains nearly unaffected along the entire reaction coordinate.
- (c) Both channels C and D are initiated by the *gauche*-H₂Fe(CO)₃ reagent and are branched at later stages of the reaction. All species involved in these reaction channels contain an angular Fe(CO)₃ fragment (structural motif) consisting of three orthogonal to each other Fe-CO bonds within a quadratic pyramidal or octahedral iron-polyhedron.
- (d) The combination of ethylene with different iron carbonyl dihydrides provides the opportunity to examine the formation and subsequent reactions of structurally diverse π -complex adducts generally described as H₂Fe(CO)₃(η^2 -C₂H₄). The adducts undergo isomerization via TS1i transition states, where i indicates the reaction channel (A, B, C, or D), to form various ethyl monohydrides with the brutto formula of HFe(CO)₃(C₂H₅).
- (e) Three basic ethyl monohydrides are identified containing strong agostic bonds between a β H-atom of the coordinatively bound ethyl group and the iron center (M-H-C agostic bond) at various locations within the iron-centered polyhedron. They are denoted HFe(CO)₃(C₂H₅)-*eqax*, HFe(CO)₃(C₂H₅)-*axe*q, and HFe(CO)₃(C₂H₅)-*eque*q, depending on the positions of the coordinatively and agostically bound carbon atoms of the "bidentate" ethyl groups. The position of the coordinative bond of the ethyl group is indicated first in the suffixes *eque*q, *eqax*, and *axe*q. The stabilization energy of the agostic bonds are evaluated to be in the range 7–12 kcal mol⁻¹. There are additional barriers for their formation and isomerization. The internal rotation of the ethyl group in HFe(CO)₃(C₂H₅)-*axe*q of channel A, for instance, breaks the agostic bond via a barrier height 11.1 kcal mol⁻¹ to form a higher by ca. 8 kcal mol⁻¹ nonagostic isomer. The stabilization energy is somewhat higher when the initial isomer contains an angular Fe(CO)₃ moiety. It is equal to 11.5 kcal mol⁻¹ for channel D with an agostic bond energy being 6.6 kcal mol⁻¹. The higher energy isomer, identified by Weitz and co-workers,⁵⁸ also contains an agostic bond (Figure 5), which is somewhat weaker than the above ones because it connects the metal center to an α H-atom of ethylene, thus creating a larger ring-strain for the bidentate ligation

- of $-\text{C}_2\text{H}_5$ group and increased interligand repulsions.⁹³ For this reason, it cannot occupy a separate open ligand site and increase the local symmetry of the iron polyhedron, as agostic bonds linked by βH -atoms identified by us do. We refer to αH type of bonds as “partial” agostic bonds. The formation of higher symmetry βH -atom bound intermediates provides the theoretical basis for the explanation of the diversity of reaction channels suggested in this paper. The agostic bond between an open site of the metallocomplex and a hydrogen atom of the attached ligand can effectively shield the potential reactive site, which requires the scission of the agostic bond prior to a new ligand attachment.
- (f) There are two competitive pathways to ethane formation: (i) a monomolecular reaction via the transition-state TS2i and (ii) a bimolecular reaction via the transition-state TS3i. All ethyl monohydride intermediates $\text{HFe}(\text{CO})_3(\text{C}_2\text{H}_5)$ lead to the reductive elimination of C_2H_6 via TS2i, either by direct means (through channels B and C) or through additional rotation barriers, which rearrange sterically the isomers (channels A and D). Channel C constitutes the most suitable pathway for the direct formation of ethane in the gas-phase reactions. The low-energy profile of the reactions involved in channel C explains the suggestion of Weitz et al.⁵⁸ that direct reductive elimination of ethane is possible without involving a second ethylene. A monomolecular reaction can readily occur when the adduct is energized either by photochemical means or via chemical activation (due to the large well depth of the initial association reaction). An easy coproduction of $\text{Fe}(\text{CO})_3$ via TS2i can explain the high turnover number of ethane production (~ 5) defined as the ratio between the concentration of produced ethane and the concentration of $\text{Fe}(\text{CO})_3$, the catalytic precursor.³³ In addition, the experimentally detected increase in the turnover number with temperature is in agreement with the expected increase in the rate of the monomolecular reactions.
- (g) The second olefin assisted (bimolecular) reaction via TS3i, which leads to $\text{Fe}(\text{CO})_3(\eta^2\text{-C}_2\text{H}_4) + \text{C}_2\text{H}_6$, can evidently occur via channels B and C but is unlikely to occur via channel D, because the latter involves a high initial rotation barrier and a shallow minimum, which does not allow the intermediate to become sufficiently stabilized to add a second ethylene molecule. The process also does not occur via channel A whereas it is favored by channel B, which involves the transition-state TS3B. The ethyl monohydride intermediate faces a high forward TS2B barrier ($24.6 \text{ kcal mol}^{-1}$) being partly stabilized by equilibrium with the initial dihydride adduct due to the low isomerization barrier, which allows the adding of a second C_2H_4 . It is important to note that the adduct $\text{HFe}(\text{CO})_3(\text{C}_2\text{H}_5)(\eta^2\text{-C}_2\text{H}_4)$ containing the second olefin, generates a nonreactive σ -complex $\text{Fe}(\text{CO})_3(\text{C}_2\text{H}_5)_2$ via a small activation barrier.
- (h) The identification of hydrogenated intermediate complexes in photochemical conditions is very demanding and there is no detailed information regarding the roles of the different isomers. All stereoisomer hydrides (even the high energy ones) have some probabilities to trigger reaction channels. A reaction channel can start from

either of the two singlet- and two triplet-state dihydrogen reagent complexes and merge into the original pathway before a product formation barrier arises. However, the triplet ${}^3\text{Fe}(\text{CO})_3(\text{H}_2)$ cannot directly react with ethylene to produce the hydrogenated compounds because of the repulsive character of the triplet PES, particularly at the entrance region of the channel. It must undergo an initial intersystem crossing before advancing the process.

- (i) The singlet PES produces the singlet $\text{Fe}(\text{CO})_3$ via TS2i. The singlet $\text{HFe}(\text{CO})_3(\text{C}_2\text{H}_5)\text{-axeq}$ intermediate can form its triplet counterpart within channel B via a vertical excitation energy of $15.9 \text{ kcal mol}^{-1}$ followed by the generation of ${}^3\text{Fe}(\text{CO})_3$ through a straightforward triplet barrier of activation (ca. 6 kcal mol^{-1}). This triplet barrier is somewhat lower than the corresponding singlet barrier TS2B (by $2.4 \text{ kcal mol}^{-1}$). Such a process can occur via the photochemical excitation of adduct. Being formed from the high energy *cis*-dihydrido reagent, the singlet adduct can be sufficiently energized.

To validate the developed elementary reaction network, and completely characterize the kinetics of olefin hydrogenation, it is necessary to determine the rate constants of all relevant reactions. The ongoing work includes further analysis of the molecular mechanisms and the development of a network of radical reactions to create a combined detailed pressure-dependent gas-phase kinetic model.

IV. CONCLUSIONS

A detailed mechanistic analysis is reported for the hydrogenation of ethylene by photoactivated $\text{Fe}(\text{CO})_5$ based on a comprehensive potential energy surface.

Four reaction channels (denoted A, B, C, and D) are identified corresponding to four PES-cross sections (Figures 2, 4, 6, and 7) involving the combination and subsequent reactions of ethylene molecule with three distinct singlet-state dihydride stereoisomers: (A) *trans*- $\text{H}_2\text{Fe}(\text{CO})_3$, (B) *cis*- $\text{H}_2\text{Fe}(\text{CO})_3$, and (C)/(D) *gauche*- $\text{H}_2\text{Fe}(\text{CO})_3$. There are two singlet-state and two triplet-state dihydrogen complexes (two of them identified for the first time) that can alternatively coordinate ethylene and trigger its hydrogenation. However, to produce ethane, they must first transform into their dihydride counterparts, or to produce triplet reagents, undergo intersystem crossings, and then follow the singlet dihydride surface (A, B, C, or D). A systematic and comprehensive examination of the actual pathways has been performed and all relevant stationary points along the reaction coordinates identified.

It is demonstrated that various interconversions precede the product formation pathways and play decisive roles in the reductive elimination of ethane. The interconversion processes (primarily hydridic H-transfer to ethylene and internal rotations of the formed ethyl group, C_2H_4 , and H_2 ligands) are found to be rate-determining steps for some catalytic cycles, which should be taken into account in the derivation of the rate laws.

There are significant variations in the barrier heights for both the direct elimination and second- C_2H_4 -addition channels, which are dependent on the symmetry of the initial reagents.

The DFT-calculated structures of π -dihydrides and σ -ethyl monohydrides together with identified reaction barriers explain the different reactivity of the isomeric reagents. Three types of monohydrides have been identified. The first type involves a strong agostic shielding of a reactive site by a metal bound H-

atom of the terminal methyl group, which occupies a vacant position in the iron polyhedron. The other two types of monohydrides either do not contain agostic bonds or contain those that do not alter the polyhedra (we refer to those as “partial” agostic bonds). An agostic bond substantially stabilizes an intermediate complex ($\sim 8\text{--}12 \text{ kcal mol}^{-1}$), thus affecting the direction of the reaction. The agostic-ligated intermediates require either the scission of the agostic bonds prior to the attachment of the second ethylene (to surpass TS3i), or the steric rearrangements allowing the reductive elimination of ethane via the monomolecular transition-state TS2i. The agostic shield particularly reduces the barrier TS2C by stabilizing the transition state.

The PES analysis revealed that the monomolecular direct elimination of ethane can well compete with the bimolecular second-C₂H₄-addition reaction in certain conditions. It can occur more efficiently when the intramolecular energy rearrangement of vibrationally excited iron carbonyls is faster than the intermolecular energy dissipation, as it takes place during the photolysis of Fe(CO)₅ at specific wavelengths.⁴

The stereospecific mechanistic results and calculated thermochemical and structural parameters constitute a basis for further developing of detailed gas-phase pressure-dependent kinetics models for iron–carbonyl catalysis and evaluating the phase-specific pathways. The dissociation of energized molecules (either photochemically or chemically) is best described by RRKM, or the modified quantum RRK theories for $k(T,P)$ and the Master Equation for falloff, for which the energy profiles constitute the most challenging issues (see, e.g., refs 26, 54–57, 91, and 92).

■ ASSOCIATED CONTENT

Supporting Information

Calculated geometries and frequencies for all stationary points and complete ref 84. This material is available free of charge via the Internet at <http://pubs.acs.org>.

■ AUTHOR INFORMATION

Notes

The authors declare no competing financial interest.

[†]Detailed theoretical analysis of free radical pathways is the topic of a subsequent publication.

■ ACKNOWLEDGMENTS

This work was supported in part by the Ruckenstein fund (University at Buffalo, SUNY). We acknowledge CCR UB providing the High Performance Computing resources. We thank also the reviewers for valuable comments.

■ REFERENCES

- (1) Geoffroy, G. L.; Wrighton, M. S. *Organometallic Photochemistry*; Academic: New York, 1979.
- (2) Chirik, P. J. Modern Alchemy: Replacing Precious Metals with Iron in Catalytic Alkene and Carbonyl Hydrogenation Reactions. In *Catalysis without Precious Metals*; Bullock, R. M., Ed.; Wiley-VCH Verlag: Berlin, Germany, 2010; Chapter 4.
- (3) Weitz, E. Transient Infrared Spectroscopy as a Probe of Coordinatively Unsaturated Metal Carbonyls in the Gas Phase. *J. Phys. Chem.* **1994**, *98*, 11256–11264.
- (4) Leadbeater, N. Enlightening Organometallic Chemistry: the Photochemistry of Fe(CO)₅ and the Reaction Chemistry of Unsaturated Iron Carbonyl Fragments. *Coord. Chem. Rev.* **1999**, *188*, 35–70.

- (5) Rabek, J. F. *Progress in Photochemistry and Photophysics*; CRC Press: Boca Raton, FL, 1990; Vol. 1.
- (6) Babich, I. M.; Garcia, R. R. P. Olefin Hydrogenation with Iron Carbonyls as Catalyst. *J. Braz. Chem. Soc.* **1997**, *8*, 215–218.
- (7) Flückiger, M. Iron(II) in Asymmetric Hydrosilylation. *Dissertation*, ETH Zurich, 2011.
- (8) Nakazawa, H.; Itazaki, M. Fe-H Complexes in Catalysis. *Top. Organomet. Chem.* **2011**, *33*, 27–81.
- (9) Krusic, P. J.; Jones, D. J.; Roe, D. C. Photochemical Activation of Molecular Hydrogen by Fe(CO)₅. *Organometallics* **1986**, *5*, 456–460.
- (10) Cais, M.; Maoz, N. Organometallic Studies. Part XXXIII. Hydrogenation of Olefins and Ligand Exchange Reactions Catalysed by Iron Carbonyl Complexes. *J. Chem. Soc. A* **1971**, 1811–1820.
- (11) Sánchez-Delgado, R. A.; Rosales, M. Kinetic Studies as a Tool for the Elucidation of the Mechanisms of Metal Complex-Catalyzed Homogeneous Hydrogenation Reactions. *Coord. Chem. Rev.* **2000**, *196*, 249–280.
- (12) Arndtsev, B. A.; Bergman, R. G.; Mobley, T. A.; Peterson, T. H. Selective Intermolecular Carbon–Hydrogen Bond Activation by Synthetic Metal Complexes in Homogeneous Solution. *Acc. Chem. Res.* **1995**, *28*, 154–162.
- (13) Torrent, M.; Sola, M.; Frenking, G. Theoretical Study of Gas-Phase Reactions of Fe(CO)₅ with OH⁻ and Their Relevance for the Water Gas Shift Reaction. *Organometallics* **1999**, *18*, 2801–2812.
- (14) Herman, I. P. Laser Deposition of Thin Films from Gas-Phase and Adsorbed Molecules. *Chem. Rev.* **1989**, *89*, 1323–1357.
- (15) Kuo, D.-H.; Su, M.-Y. The Effects of Hydrogen and Temperature on the Growth and Microstructure of Carbon Nanotubes Obtained by the Fe(CO)₅ Gas-Phase-Catalytic Chemical Vapor Deposition. *Surf. Coatings Technol.* **2007**, *201*, 9172–9178.
- (16) Hill, H. G. M.; Nuth, J. A. The Catalytic Potential of Cosmic Dust. *Astrobiology* **2003**, *3*, 291–304.
- (17) Harvey, J. N.; Poli, R. Computational Study of the Spin-Forbidden H₂ Oxidative Addition to 16-electron Fe(0) Complexes. *Dalton Trans.* **2003**, 4100–4106.
- (18) Crabtree, R. H. *The Organometallic Chemistry of the Transition Metals*, 5th ed.; John Wiley & Sons: Hoboken, NJ, 2009.
- (19) Kubas, G. J. *Metal Dihydrogen and Sigma-Bond Complexes Structure, Theory, and Reactivity*; Springer: Berlin, 2001.
- (20) Gordon, J. C.; Kubas, G. J. Perspectives on How Nature Employs the Principles of Organometallic Chemistry in Dihydrogen Activation in Hydrogenases. *Organometallics* **2010**, *29*, 4682–4701.
- (21) Custelcean, R.; Jackson, J. E. Dihydrogen Bonding: Structures, Energetics, and Dynamics. *Chem. Rev.* **2001**, *201*, 1963–1980.
- (22) Epstein, L. M.; Shubina, E. S. New types of hydrogen bonding in organometallic chemistry. *Coord. Chem. Rev.* **2002**, *231*, 165–181.
- (23) Sushumna, I.; Ruckenstein, E. Role of Physical and Chemical Interactions on the Behavior of Supported Metal Catalysts: Iron on Alumina - A Case Study. *J. Catal.* **1985**, *94*, 239–288.
- (24) Asatryan, R. Molecular Hydrogen Assisted Transport of H-atoms. *Chem. Phys. Lett.* **2010**, *498*, 263–269.
- (25) Asatryan, R.; Bozzelli, J. W.; Ruckenstein, E. Dihydrogen Catalysis: A Degradation Mechanism for N₂-Fixation Intermediates. *J. Phys. Chem. A* **2012**, *116*, 11618–11642.
- (26) Asatryan, R.; Bozzelli, J. W.; da Silva, G.; Swinnen, S.; Nguyen, M. T. Formation and Decomposition of Chemically Activated and Stabilized Hydrazine. *J. Phys. Chem. A* **2010**, *114*, 6235–6249.
- (27) Poliakoff, M.; Weitz, E. Shedding Light on Organometallic Reactions: the Characterization of Tetracarbonyliron (Fe(CO)₄), a Prototypical Reaction Intermediate. *Acc. Chem. Res.* **1987**, *20*, 408–414.
- (28) Schroeder, M. A.; Wrighton, M. S. Pentacarbonyliron(0) Photocatalyzed Reactions of Trialkylsilanes with Alkenes. *J. Am. Chem. Soc.* **1976**, *98*, 551–558.
- (29) Miller, M. E.; Grant, E. R. Relaxation Kinetics in the Homogeneous Gas-Phase Photocatalytic Hydrogenation of Ethylene by Fe(CO)₄(C₂H₄). *J. Am. Chem. Soc.* **1984**, *106*, 4635–4636.

- (30) Miller, M. E.; Grant, E. R. Gas-Phase Organometallic Catalysis: Kinetics and Mechanism of the Hydrogenation of Ethylene by $\text{Fe}(\text{CO})_3(\text{C}_2\text{H}_4)_2$. *J. Am. Chem. Soc.* **1987**, *109*, 7951–7960.
- (31) Miller, M. E.; Grant, E. R. Energetics of a Homogeneous Gas-phase Photocatalytic System: the Hydrogenation of Ethylene by $\text{Fe}(\text{CO})_4(\text{C}_2\text{H}_4)$. *J. Am. Chem. Soc.* **1985**, *107*, 3386–3387.
- (32) Hayes, D. M.; Weitz, E. A Study of the Kinetics of Reaction of $\text{Fe}(\text{CO})_3$ and $\text{Fe}(\text{CO})_3(\text{L})$ with H_2 and C_2H_4 for $\text{L} = \text{H}_2$ and C_2H_4 by Transient Infrared Spectroscopy: Reactions Relevant to Olefin Hydrogenation Kinetics. *J. Phys. Chem.* **1991**, *95*, 2723–2727.
- (33) Wells, J. R.; Weitz, E. A Time-Resolved Fourier Transform Infrared Study of the Catalytic Hydrogenation of C_2H_4 Following UV Photolysis of Mixtures of $\text{Fe}(\text{CO})_5$, C_2H_4 , and H_2 . *J. Phys. Chem.* **1993**, *97*, 3084–3087.
- (34) Poliakoff, M.; Turner, J. J. The Structure of $[\text{Fe}(\text{CO})_4]$ -An Important New Chapter in a Long-Running Story. *Angew. Chem., Int. Ed.* **2001**, *40*, 2809–2812.
- (35) Ihee, H.; Cao, J.; Zewail, A. H. Ultrafast Electron Diffraction of Transient $[\text{Fe}(\text{CO})_4]$: Determination of Molecular Structure and Reaction Pathway. *Angew. Chem.* **2001**, *113*, 1580–1584.
- (36) Mitchener, J. C.; Wrighton, M. S. Low-temperature Photochemistry of Tetracarbonylethyleneiron and Tetracarbonylpropyleneiron. Spectroscopic Observation of Catalytically Significant Intermediates. *J. Am. Chem. Soc.* **1983**, *105*, 1065–1067.
- (37) Long, G. T.; Weitz, E. A Study of the Mechanism of Iron Carbonyl-Catalyzed Isomerization of 1-Pentene in the Gas Phase using Time-Resolved Infrared Spectroscopy. *J. Am. Chem. Soc.* **2000**, *122*, 1431–1442.
- (38) Long, G. T.; Wang, W.; Weitz, E. A Real Time Spectroscopic Probe of P-Hydrogen Transfer in the Gas Phase: Formation of $\text{HFe}(\text{CO})_3(\eta^3\text{-C}_3\text{H}_5)$. *J. Am. Chem. Soc.* **1995**, *117*, 12810–12818.
- (39) Cedeño, D. L.; Weitz, E. Density Functional Theory Study of $\text{Fe}(\text{CO})_3(\eta^2\text{-C}_3\text{H}_6)$, $\text{HFe}(\text{CO})_3(\eta^3\text{-C}_3\text{H}_5)$, and the Iron-allyl Bond Energy. *Organometallics* **2003**, *22*, 2652–2659.
- (40) Fleckner, H.; Grevels, F.-W.; Hess, D. Tricarbonylbis(η -2-Cis-Cyclooctene)Iron: Photochemical Synthesis of a Versatile Tricarbonyliron Source for Olefin Isomerization and Preparative Applications. *J. Am. Chem. Soc.* **1984**, *106*, 2027–2032.
- (41) Ellerhorst, G.; Gerhardt, W.; Grevels, F.-W. Low-Temperature Matrix Photochemistry of (1,3-Diene)Tricarbonyliron Complexes. *Inorg. Chem.* **1980**, *19*, 67–71.
- (42) Snee, P. T.; Payne, C. K.; Mebane, S. D.; Kotz, K. T.; Harris, C. B. Dynamics of Photosubstitution Reactions of $\text{Fe}(\text{CO})_5$, An Ultrafast Infrared Study of High Spin Reactivity. *J. Am. Chem. Soc.* **2001**, *123*, 6909–6915.
- (43) Ryther, R. J.; Weitz, E. Reaction Kinetics of Coordinatively Unsaturated Iron Carbonyls Formed on Gas-Phase Excimer Laser Photolysis of $\text{Fe}(\text{CO})_5$. *J. Phys. Chem.* **1991**, *95*, 9841–9852.
- (44) Ryther, R. J.; Weitz, E. Diode Laser Probes of the Product Distribution of Coordinatively Unsaturated Iron Carbonyls Produced Following Excimer Laser Photolysis of $\text{Fe}(\text{CO})_5$ in the Gas Phase. *J. Phys. Chem.* **1992**, *96*, 2561–2567.
- (45) González-Blanco, O.; Branchadell, V. Density functional study of the Fe–CO bond dissociation energies of $\text{Fe}(\text{CO})_5$. *J. Chem. Phys.* **1999**, *110*, 778–7843.
- (46) Bachler, V.; Grevels, F. W.; Kerpen, K.; Olbrich, G.; Schaffner, K. A Novel Facet of Carbonyliron-Diene Photochemistry: The η^4 -s-trans Isomer of the Classical $\text{Fe}(\text{CO})_3(\eta^4\text{-s-cis-1,3-butadiene})$ Discovered by Time-Resolved IR Spectroscopy and Theoretically Examined by Density Functional Methods. *Organometallics* **2003**, *22*, 1696–1711.
- (47) Nguyen, S. C.; Lomont, J. P.; Zoerb, M. C.; Hill, A. D.; Schlegel, J. P.; Harris, C. B. Chemistry of the Triplet 14-electron Complex $\text{Fe}(\text{CO})_3$ in Solution Studied by Ultrafast Time-resolved IR Spectroscopy. *Organometallics* **2012**, *31*, 3980–3984.
- (48) Schröder, D.; Shaik, S.; Schwarz, H. Two-State Reactivity as a new Concept in Organometallic Chemistry. *Acc. Chem. Res.* **2000**, *33*, 139–145.
- (49) Besora, M.; Carreón-Macedo, J.-L.; Cowan, A. J.; George, M. W.; Harvey, J. N.; Portius, P.; Ronayne, K. L.; Sun, X.-Zh.; Towrie, M. A Combined Theoretical and Experimental Study on the Role of Spin States in the Chemistry of $\text{Fe}(\text{CO})_5$ Photoproducts. *J. Am. Chem. Soc.* **2009**, *131*, 3583–3592.
- (50) Smirnov, V. N. Thermal Dissociation and Bond Energies of Iron Carbonyls $\text{Fe}(\text{CO})_n$ ($n = 1$ – 5). *Kinetics and Catalysis* **1993**, *34*, 591–598.
- (51) Waller, I. M.; Hepburn, J. W. State-Resolved Photofragmentation Dynamics of $\text{Fe}(\text{CO})_5$ at 193, 248, 266, and 351 nm. *J. Chem. Phys.* **1988**, *88*, 6658–6669.
- (52) Wen, J. Z.; Franklin Goldsmith, C.; Ashcraft, R. W.; Green, W. H. Detailed Kinetic Modeling of Iron Nanoparticle Synthesis from the Decomposition of $\text{Fe}(\text{CO})_5$. *J. Phys. Chem. C* **2007**, *111*, 5677–5688.
- (53) Halpern, J. Mechanism and Stereoselectivity of Asymmetric Hydrogenation. *Science* **1982**, *217*, 4558–4559.
- (54) Asatryan, R.; Bozzelli, J. W. Chain Branching and Termination in Low Temperature Combustion of *n*-Alkanes. *J. Phys. Chem. A* **2010**, *114*, 7693–7708.
- (55) Asatryan, R.; da Silva, G.; Bozzelli, J. W. Quantum Chemical Study of the Acrolein (CH_2CHCHO) + $\text{OH} + \text{O}_2$ Reactions. *J. Phys. Chem. A* **2010**, *114*, 8302–8311.
- (56) Bozzelli, J. W.; Asatryan, R.; Montgomery, C. J.; Sheng, C. Pressure-Dependent Mechanism for H/O/C(1) Chemistry. *Proceedings of the 5th US National Meeting on Combustion*, March 2007, San Diego, USA; Combustion Institute: Pittsburgh, PA, 2007.
- (57) Chang, A. Y.; Bozzelli, J. W.; Dean, A. M. Kinetic Analysis of Complex Chemical Activation and Unimolecular Dissociation Reactions Using QRRK Theory and the Modified Strong Collision Approximation. *Z. Phys. Chem.* **2000**, *214*, 1533–1568.
- (58) Kismartoní, L. C.; Weitz, E.; Cedeño, D. L. Density Functional Study of $\text{Fe}(\text{CO})_3$ and $\text{Fe}(\text{CO})_3(\text{L})$ with H_2 and C_2H_4 , where $\text{L} = \text{H}_2$ or C_2H_4 : Reactions Relevant to Olefin Hydrogenation. *Organometallics* **2005**, *24*, 4714–4720.
- (59) Onda, K.; Takahashi, M.; Ishikawa, Y.; Sugita, K.; Tanaka, K.; Arai, S.; Rayner, D. M.; Hackett, P. A. Mechanism of Hydrogenation of Ethylene via Photoproduced Unsaturated Iron Carbonyl in the Gas Phase. *J. Phys. Chem.* **1991**, *95*, 758–761.
- (60) Nagorski, H.; Mirbach, M. J. A Radical Mechanism for the Photochemical Iron Pentacarbonyl Catalyzed Hydrogenation of Octenes. *J. Organomet. Chem.* **1985**, *291*, 199–204.
- (61) Belousov, Yu. A. Radical Chemistry of Iron Carbonyls. *Russ. Chem. Rev.* **2007**, *76*, 41–58.
- (62) Becke, A. Density-Functional Thermochemistry. III. The Role of Exact Exchange. *J. Chem. Phys.* **1993**, *98*, 5648–5652.
- (63) Lee, C.; Yang, W.; Parr, R. G. Development of the Colle-Salvetti Correlation-Energy Formula into a Functional of the Electron Density. *Phys. Rev. B* **1988**, *37*, 785–789.
- (64) Stephens, P. J.; Devlin, F. J.; Chabalowski, C.; Frisch, M. J. Ab Initio Calculation of Vibrational Absorption and Circular Dichroism Spectra Using Density Functional Force. *J. Phys. Chem.* **1994**, *98*, 11623–11627.
- (65) Perdew, L. P.; Wang, Y. Accurate and Simple Analytic Representation of the Electron-Gas Correlation Energy. *Phys. Rev. B* **1992**, *45*, 13244–13249.
- (66) Hirva, P.; Haukka, M.; Jakonen, M. DFT Tests for Group 8 Transition Metal Carbonyl Complexes. *J. Mol. Model.* **2008**, *14*, 171–181.
- (67) Paier, J.; Marsman, M.; Kresse, G. Why does the B3LYP Hybrid Functional fail for Metals? *J. Chem. Phys.* **2007**, *127*, 024103–1–10.
- (68) Simón, L.; Goodman, J. M. How Reliable are DFT Transition Structures? Comparison of GGA, Hybrid-Meta-GGA and Meta-GGA Functionals. *Org. Biomol. Chem.* **2011**, *9*, 689–700.
- (69) Asatryan, R.; Bozzelli, J. W. Formation of Criegee Intermediate in Low Temperature Oxidation of Dimethyl Sulfoxide. *Chem. Phys. Phys. Chem.* **2008**, *10*, 1769–1780.
- (70) Izgorodina, E. I.; Brittain, D. R. B.; Hodgson, J. L.; Krenske, E. H.; Lin, C. Y.; Namazian, M.; Coote, M. L. Should Contemporary Density Functional Theory Methods be used to Study the

- Thermodynamics of Radical Reactions? *J. Phys. Chem. A* **2007**, *111*, 10754–10768.
- (71) Holthausen, M. C.; Fiedler, A.; Schwarz, H.; Koch, W. How Does Fe^+ Activate C–C and C–H Bonds in Ethane? A Theoretical Investigation Using Density Functional Theory. *J. Phys. Chem.* **1996**, *100*, 6236–6242.
- (72) Kolboe, S.; Svelle, S. Does an Ethene/Benzenium Ion Complex Exist? A Discrepancy between B3LYP and MP2 Predictions. *J. Phys. Chem. Lett.* **2008**, *112*, 6399–6400.
- (73) Basch, H.; Hoz, S. Ab Initio Study of Hydrogen Abstraction Reactions. *J. Phys. Chem. A* **1997**, *101*, 4416–4431.
- (74) Siegbahn, P. E. M. The Performance of Hybrid DFT for Mechanisms Involving Transition Metal Complexes in Enzymes. *J. Biol. Inorg. Chem.* **2006**, *11*, 695–701.
- (75) Schultz, N. E.; Zhao, Y.; Truhlar, D. G. Density Functionals for Inorganometallic and Organometallic Chemistry. *J. Phys. Chem. A* **2005**, *109*, 11127–11143.
- (76) Reiher, M.; Salomon, O.; Hess, B. A. Reparameterization of Hybrid Functionals Based on Energy Differences of States of Different Multiplicity. *Theor. Chem. Acc.* **2001**, *107*, 48–55.
- (77) Chaloner, P. A.; Esteruelas, M. A.; Joo, F.; Oro, L. A. *Homogeneous Hydrogenation*; Kluwer Academic: Dordrecht, Netherlands, 1994.
- (78) Niu, S.; Hall, M. B. Theoretical Calculations on Reactions of Transition Metal Complexes. *Chem. Rev.* **2000**, *100*, 353–406.
- (79) Wang, W.; Weitz, E. A Theoretical Study of the Reaction: $\text{H}_2 + \text{Fe}(\text{CO})_4 \rightarrow \text{H}_2\text{Fe}(\text{CO})_4$. *J. Phys. Chem. A* **1997**, *101*, 2358–2363.
- (80) Soubra, C.; Oishi, Y.; Albright, T. A.; Fujimoto, H. Intramolecular Rearrangements in Six-Coordinate Ruthenium and Iron Dihydrides. *Inorg. Chem.* **2001**, *40*, 620–627.
- (81) Asatryan, R.; Bozzelli, J. W.; Simmie, J. M. Thermochemistry of Methyl and Ethyl Nitro, $\text{R}-\text{NO}_2$, and Nitrite, RONO , Organic Compounds. *J. Phys. Chem. A* **2008**, *112*, 3172–3185.
- (82) Dunning, T. H., Jr.; Hay, P. J. In *Modern Theoretical Chemistry*; Schaefer, H.F., III, Ed.; Plenum Press: New York, 1976; Vol. 3, pp 1–28.
- (83) Hay, P. J.; Wadt, W. R. Ab initio Effective Core Potentials for Molecular Calculations. Potentials for K to Au Including the Outermost Core Orbitals. *J. Chem. Phys.* **1985**, *82*, 299–310.
- (84) Frisch, M. J.; Trucks, G. W.; Schlegel, H. B.; Scuseria, G. E.; Robb, M. A.; Cheeseman, J. R.; Montgomery, J. A., Jr.; Vreven, T.; Kudin, K. N.; Burant, J. C.; et al. *Gaussian 03*, Rev. D.01; Gaussian, Inc.: Wallingford, CT, 2004.
- (85) Dolg, M.; Wedig, U.; Stoll, H.; Preuss, H. Energy-Adjusted Ab initio Pseudopotentials for the First Row Transition Elements. *J. Chem. Phys.* **1987**, *86*, 866–872.
- (86) Poli, R.; Harvey, J. N. Spin Forbidden Chemical Reactions of Transition Metal Compounds. New Ideas and New Computational Challenges. *Chem. Soc. Rev.* **2003**, *32*, 1–8.
- (87) Clot, E.; Einstein, O. *Principles and Applications of Density Functional Theory in Inorganic Chemistry II*; Springer: Berlin, Germany, 2004.
- (88) Glascoe, E. A.; Kling, M. F.; Shanoski, J. E.; DiStasio, R. A., Jr.; Payne, C. K.; Mork, B. V.; Tilley, T. D.; Harris, C. B. Photoinduced Beta-Hydrogen Elimination and Radical Formation with $\text{CpW}(\text{CO})_3(\text{CH}_2\text{CH}_3)$: Ultrafast IR and DFT Studies. *Organometallics* **2007**, *26*, 1424–1432.
- (89) Sawyer, K. R.; Glascoe, E. A.; Cahoon, J. F.; Schlegel, J. P.; Harris, C. B. The Mechanism of Iron-Catalyzed Alkene Isomerization in Solution. *Organometallics* **2008**, *27*, 4370–4379.
- (90) Three possible mechanisms for decay of ${}^3\text{Fe}(\text{CO})_3(\text{H}_2)$ were considered in ref 49: (a) spin-state change of ${}^3\text{Fe}(\text{CO})_3(\text{H}_2)$ to ${}^1\text{Fe}(\text{CO})_3(\text{H}_2)$ or ${}^1\text{Fe}(\text{CO})_3(\text{H})_2$, followed by the rapid addition of CO, (b) direct spin-forbidden addition of CO to ${}^3\text{Fe}(\text{CO})_3(\text{H}_2)$, and (c) spin-allowed reaction between CO and ${}^3\text{Fe}(\text{CO})_3(\text{H}_2)$ to give ${}^3\text{Fe}(\text{CO})_3$ and H_2 . The last reaction was presumed to occur with higher probability and no direct MECP being located leading to the more stable dihydride species. See also: Besora, M.; Carreón-Macedo, J.-L.; Cimas, Á.; Harvey, J. N. Spin-state changes and reactivity in transition metal chemistry: Reactivity of iron tetracarbonyl. *Adv. Inorg. Chem.* **2009**, *61*, 573–623.
- (91) Jin, F.; Asatryan, R.; Bozzelli, J. W. Thermodynamic and Kinetic Analysis of the Activation Reaction of Dimethyl Sulfide Radical with Oxygen. *Int. J. Quantum Chem.* **2012**, *112*, 1945–1958.
- (92) da Silva, G.; Bozzelli, J. W.; Asatryan, R. Hydroxyl Radical Initiated Oxidation of *s*-Triazine: Hydrogen Abstraction is Faster than Hydroxyl Addition. *J. Phys. Chem. A* **2009**, *113*, 8596–8606.
- (93) Dashevskii, V. G.; Asatryan, R.; Baranov, A. P. Interligand Interaction and the Three-Dimensional Structure of Coordination Compounds. Compounds of the Tris (bidentate) M type. *J. Struct. Chem.* **1978**, *19*, 678–686.